REVIEWS

Journal of Semiconductors
(2020) 41, 081001
doi: 10.1088/1674-4926/41/8/081001

Physical vapor deposited 2D bismuth for CMOS technology

Hanliu Zhao[1, ‡], Xinghao Sun[1, ‡], Zhengrui Zhu[1, ‡], Wen Zhong[1], Dongdong Song[1], Weibing Lu[2, 3, †], and Li Tao[1, 2, †]

[1]School of Materials Science and Engineering, Southeast University, Nanjing 211189, China

[2]Center for Flexible RF Technology, Southeast University, Nanjing 211189, China

[3]State Key Laboratory of Millimeter Waves, School of Information Science and Engineering, Southeast University, Nanjing 211189, China

Abstract: Two-dimensional (2D) bismuth, bismuthene, is an emerging pnictogen family member that has received increasing research attention in the past few years, which could yield exotic electrical, thermal, and optical properties due to unique band structure. This review provides a holistic view of recent research advances on 2D bismuth material synthesis and device applications in complementary metal oxide semiconductor (CMOS) technology. Firstly, the atomic and band structure of bismuthene is reviewed as the fundamental understanding of its physical properties. Then, it highlights material synthesis of 2D bismuth atomic sheets with emphasis on physical vapor deposition method with accurate layer controllability and process compatibility with CMOS technology. Moreover, it will survey latest applications of 2D bismuth in terms of electronic, optic, thermoelectric, spintronic and magnetic nanodevices. 2D bismuth derivatives (Bi–X, X = Sb, Te, Se) will also be mentioned as a promising strategy to further improve device performance. At last, it concludes with a brief summary on the current challenges and future prospects in 2D bismuth and its derivatives for innovative electronics, sensors and other devices compatible with CMOS techniques.

Key words: bismuthene; 2D materials; physical vapor deposition; CMOS; nanoelectronics

Citation: H L Zhao, X H Sun, Z R Zhu, W Zhong, D D Song, W B Lu, and L Tao, Physical vapor deposited 2D bismuth for CMOS technology[J]. *J. Semicond.*, 2020, 41(8), 081001. http://doi.org/10.1088/1674-4926/41/8/081001

1. Introduction

Beginning with the successful exfoliation of monolayer graphene, two-dimensional (2D) materials, including h-BN, transition metal dichalcogenides (TMDs), Xenes and MXenes, have attracted significant interest in the past dozen years due to their unique physical and chemical properties. As a specific Xene branch, 2D atomic sheets of group VA elements possess tunable electrical, thermal, optical properties compared to their bulk state, thus having a broad prospect in the field of CMOS applications, such as field-effect transistors (FET), sensors, optoelectronics, thermoelectrics, topological insulators and so on. Group VA consists of nitrogen, phosphorus, arsenic, antimony and bismuth, all of which have a puckered or buckled layered structure except for nitrogen. Black phosphorus (BP) is the most thermodynamically stable allotrope of phosphorus under standard conditions[1], with puckered orthorhombic structure formed by a hexagonal ring, namely α phase (space group Cmca), while blue phosphorus possesses a buckled rhombohedral structure[2, 3], known as β phase (space group $R\bar{3}m$) as Fig. 1(a). For As, Sb and Bi, the most stable structure is β phase[4], which are also called gray arsenic, gray antimony and metallic bismuth.

As the most intensively studied 2D Xene material, BP is known for its tunable direct band gap (0.3 eV for bulk and ~2 eV for monolayer), anisotropic transport properties, thickness-dependent anisotropic optical response[5], and high carrier mobility (of order 10^4 cm^2 V^{-1} s^{-1} along the zigzag direction)[6], promising for nano-electronic and optoelectronic devices. At room temperature, BP FET shows a thickness-dependent mobility up to 10^3 cm^2 V^{-1} s^{-1}, and the drain current modulation is on the order of 10^5, which demonstrates the potential for CMOS device applications[7]. Nevertheless, poor air stability[8] is an obstacle for practical applications of BP, although air-stable BP devices with encapsulation have been demonstrated[9].

2D monolayer arsenene possesses carrier mobility as high as 635 cm^2 V^{-1} s^{-1} for electrons and 1700 cm^2 V^{-1} s^{-1} for holes as calculated[10]. A large indirect bandgap of ~2.49 eV for β-arsenene is also predicted[1]. Nevertheless, Pumera *et al.*[11] reported that arsenic nanosheets were considered to be nonnegligible highly toxic, which may restrict their biomedical and related applications. Monolayer β-antimonene is calculated to have an intrinsic indirect bandgap of ~2.28 eV[1, 12], and high mobility similar to arsenene[10]. Superadd good air stability, high surface activity, moderate toxicity and topological edge states, 2D antimony shows great potential in battery, topological insulators, field-effect transistors, electrocatalysis and so on[8, 11, 13–15].

As the last element of the VA group, β-bismuth possesses the same rhombohedral structure as arsenic and antimony[1, 4]. Due to the heavy atom, bulk bismuth has a strong spin-orbit coupling effect[16, 17]. And p bands cross the Fermi level at T and L points as Fig. 1(c) presented, leading to a small overlap of about 30–40 meV in the valence band and conduction band[18, 19] as shown in Fig. 1(d). Hence, bulk bis-

Hanliu Zhao, Xinghao Sun, and Zhengrui Zhu contribute equally.
Correspondence to: W B Lu, wblu@seu.edu.cn; L Tao, tao@seu.edu.cn

Received 6 JUNE 2020; Revised 6 JULY 2020.

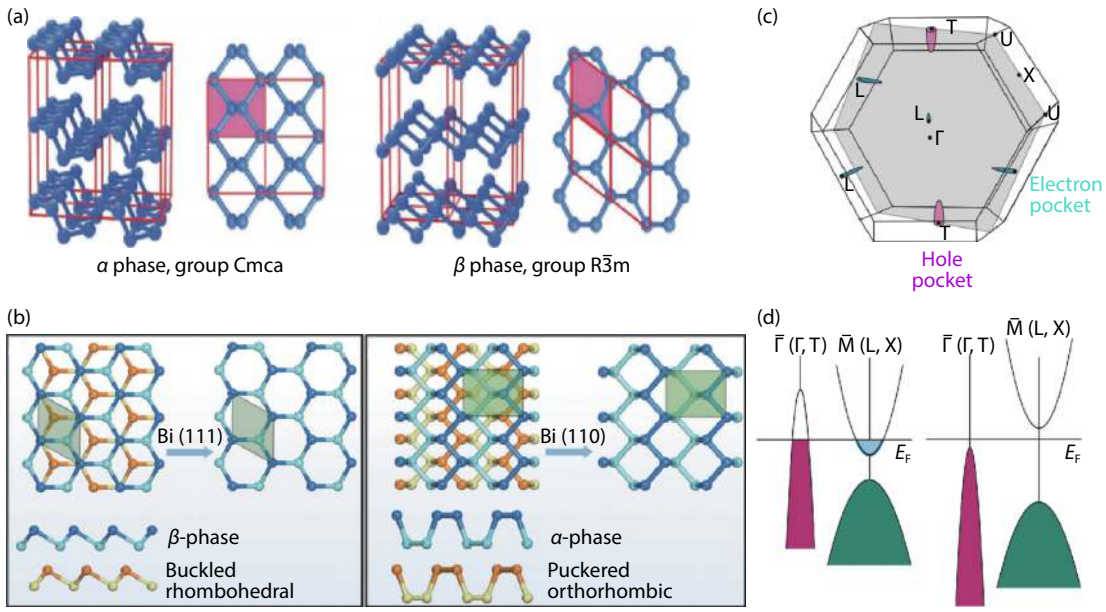

Fig. 1. (Color online) (a) Atomic structure of α phase P (left) and β phase As, Sb, Bi(right). Reproduced with permission from Ref. [4]. Copyright 2018, The Royal Society of Chemistry. (b) Top and side views of Bi(111), which exhibit a buckled honeycomb structure (left), and Bi(110), which exhibit a puckered black-phosphorus style allotrope. Reproduced with permission from Ref. [42]. Copyright 2020, The Royal Society of Chemistry. (c) Bulk Brillouin zone of Bi. Reproduced with permission from Ref. [20]. Copyright 2006, Elsevier Ltd. (d) Schematic drawing of the Bi band structure near the Fermi level at metallic (left) and semiconducting (right) phase. Reproduced with permission from Ref. [19]. Copyright 2006, American Physical Society.

muth displays metallic behavior, known as metallic bismuth. 2D bismuth exhibits a lower carrier concentration than that of normal metals[20], long Fermi wavelength results in a semimetal to semiconductor transition when the thickness is down to ~30 nm on account of the quantum size effect[21–23]. Unlike BP, the scanning electron microscope (SEM), X-ray diffraction (XRD) and Raman characterizations of vapor-deposited bismuth films did not show significant degradation after 30 days[24, 25], demonstrating their good air stability. At room temperature, 0.1–2 μm bismuth thin films show high carrier mobility up to ~2×10^4 cm^2 V^{-1} s^{-1}[26]. The small carrier effective mass (~0.001m_o) and the long mean free path can produce giant magnetoresistance effect in 2D bismuth[20, 23, 27]. Beyond that, low thermal conductivity, optical anisotropy, high catalytic activity[28], high specific capacity[29] and mild cytotoxicity[11] make it a promising candidate for future nanoelectronics.

With the rapid increase in 2D materials research, many emerging 2D materials such as graphene, BP and TMDs, have been demonstrated to be applicable to CMOS devices, including transistors, memories and inverters, benefiting from their high carrier mobility or tunable bandgap[30–33]. In general, 2D bismuth's outstanding properties in high mobility and a suitable bandgap will also qualify it for CMOS applications.

Starting from the structure and properties of bismuth, this review summarizes various physical vapor deposition of 2D bismuth, followed by its existing or potential CMOS applications. Besides, bismuth derivatives are mentioned as a strategy to enhance the performance of 2D bismuth. Finally, a brief summary on the current challenges and future prospects are discussed. Besides, it should be noted that in this review, "bismuthene" refers to bismuth from monolayer to 4 nm, "2D bismuth" indicates 4–30 nm (critical thickness for observing quantum confinement effect[20]), and "thin film" is for 30 nm or thicker bismuth.

2. Structure and properties of bismuthene

As a cousin of phosphorene, the unique structure of bismuthene gives rise to extraordinary electronic properties. To utilize the properties in potential applications, it is necessary to understand the relationship between the atomic, band structure and electronic properties of 2D bismuth.

2.1. Atomic structure

Bismuth possesses a rhombohedral A7-type structure, namely β phase as shown in Fig. 1(a), space group R$\bar{3}$m that each Bi atom is covalently bonded to three nearest-neighbor atoms and has and three next-nearest neighbors slightly further away[34]. For 2D bismuth, β-phase Bi (111) and α-phase Bi (110) are two distinctive allotropes as shown in Fig. 1(b) with similar average binding energy according to the same simulation method[4], both of which can be realized experimentally as seen in Section 3.1. Note that Bi (111) and (110) planes in the rhombohedral coordinates are equal to (003) and (012) in the hexagonal coordinates[20]. Bi (111) and (110) are reported to be topologically non-trivial and possess interesting electronic properties[35–37]. The interlayer distance is ~0.328 nm for Bi (110) planes and ~0.395 nm for Bi (111) planes according to PDF#44-1246. The lattice parameters of Bi crystal are $a = b = 4.547$ Å, $c = 11.8616$ Å, $\alpha = \beta = 90°$, $\gamma = 120°$, bond length $d = 3.07$ Å, buckling parameter $\Delta Z = 1.60$ Å. For monolayer β-bismuthene, the optimized lattice constant will slightly decrease to ~4.36 Å, and the buckling parameter will increase to ~1.73 Å[38, 39], indicating that low dimensionality has an effect on atomic structure parameters[40]. Interestingly, there is a transition from puckered (similar to

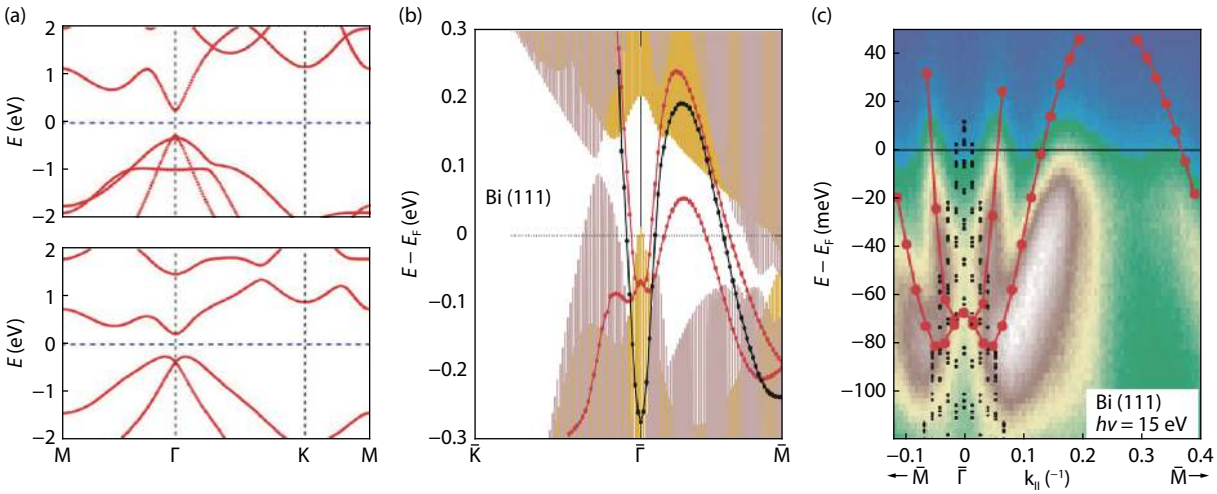

Fig. 2. (Color online) (a) Band structure of bismuthene is calculated without (up) and with (down) the SOC. Reproduced with permission from Ref. [39]. Copyright 2017, American Chemical Society. (b) Surface states of Bi (111) calculated without (black) and with (red) spin-orbit splitting included. The shaded areas show the projection of the bulk bands obtained without (violet) and with (yellow) SOC and their superposition (brown). (c) Calculated and measured electronic structure on Bi (111) surface. Reproduced with permission from Ref. [16]. Copyright 2004, American Physical Society.

BP) to buckled (similar to silicon) atomic structure once bismuthene grows thicker than 6 monolayers during the epitaxy process[41], which will be introduced later on.

2.2. Band structure and electronic properties

Bismuth has an electron configuration of $6s^2\ 6p^3$[20]. Owing to the shallow electron and hole pockets at the L and T points of the 1st Brillouin zone in bismuth, charge carriers exhibit small effective masses, a long Fermi wavelength (~30 nm), a low carrier density (3×10^{17} cm^{-3}) as well as metallic behavior. It is predictable that when the thickness of 2D bismuth decreases to tens of nanometers, quantum size effect will become significant and result in fascinating properties. To be exact, when the confinement produces enough energy to lift the overlap between valence band and conduction band, a semimetal to semiconductor transition will occur at thickness ~30 nm as experimental measurement[20, 22, 23].

In general, monolayer bismuthene possesses a moderate direct bandgap ranging from 0.43 to 0.99 eV depending on different computation methods[1, 39, 43–46], whereas bulk bismuth shows a small band overlap of 30–40 meV. Fig. 2(a) illustrates the band structure of bismuthene with or without spin-orbit coupling (SOC), and shows that strong SOC will narrow the bandgap[39]. Actually, a large topological bandgap of ~0.8 eV for monolayer bismuthene on the SiC substrate has been reported[17]. Narrow gaps of 0.4–0.5 eV are demonstrated in bismuth nanostructures including nanoflakes, nanoribbons and nanorods[47, 48].

Strong SOC effect leads to a splitting of the states in heavy Bi atoms, and the large energy difference between the $6p_{1/2}$ and $6p_{3/2}$ is 1.5 eV after splitting[20]. However, the spin degeneracy cannot be lifted in the band structure because of the inversion symmetry. As for 2D bismuth, the spin-orbit splitting will strongly affect the band structure and Fermi surface due to the broken inversion symmetry, which is different from bulk bismuth with inversion symmetry. Koroteev *et al.* showed that the spin-orbit interaction results in a strong splitting of the surface state bands and changes the surface-state dispersion and the corresponding Fermi surfaces on low-index surfaces of Bi[16]. Fig. 2(b) shows the electronic structure of Bi (111) together with the bulk band structure for the (111) surface calculated with or without SOC. Angle-resolved photoemission spectroscopy (ARPES) also agrees with the calculated strong splitting with SOC as shown in Fig. 2(c). These intriguing characteristics make 2D bismuth a promising spintronic material.

3. Physical vapor deposition of 2D bismuth

Material synthesis or growth is the first step to perform experimental study on the aforementioned exotic properties of bismuthene. To date, a number of methods have been developed to fabricate 2D bismuth, including physical vapor deposition, liquid exfoliation[11, 14, 29, 49], wet chemical synthesis[50–52] and so on. Different preparation methods have diverse impact on thickness, size, morphology, structure and properties of 2D bismuth. Recently, Liu *et al.* reviewed 2D bismuth preparation methods including liquid exfoliation and wet chemical methods[42]. Liquid exfoliation is a mature fabrication technique to obtain group VA nanosheets[4] from bulk with the assistance of sonication or aqueous shear. Wet chemical methods use a Bi-based compound as the raw material to obtain 2D bismuth through chemical reactions. The products of the two are usually small pieces and are suitable for battery materials, catalysis, biosensing and so on[14, 29, 50, 52]. Thin films applied to CMOS need to be large scale, continuous and uniform. Generally speaking, physical vapor deposition methods could yield large area pristine films with controllable scale on desired substrates, which is compatible with CMOS technology. However, there are few reviews that systematically summarized the physical vapor deposition of 2D bismuth, which brings us to the purpose of this review. Several typical physical vapor deposition methods to prepare 2D bismuth will be discussed in detail below.

3.1. Molecular beam epitaxy (MBE)

Under ultra-high vacuum (~10^{-8} Pa) and small mismatch,

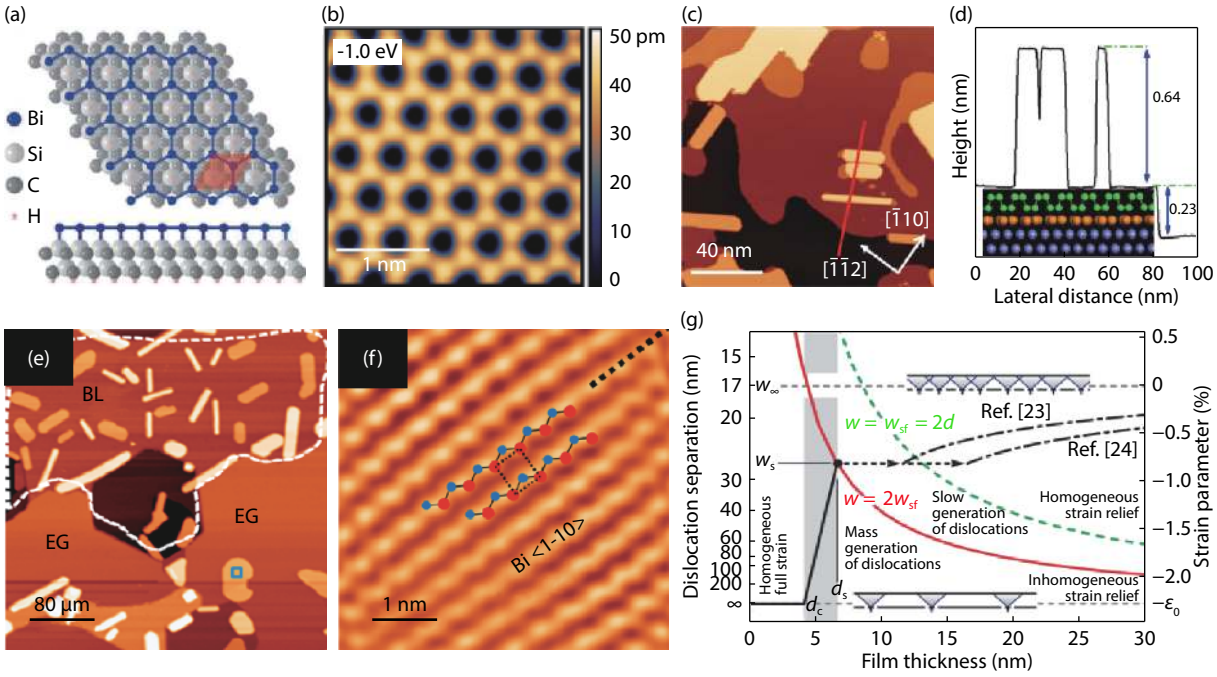

Fig. 3. (Color online) (a) Sketch and (b) STM image of flat honeycomb bismuthene epitaxy on SiC (0001). Reproduced with permission from Ref. [17]. Copyright 2020, American Association for the Advancement of Science. (c) STM image of ~ 1.2 monolayer Bi on Au (111) and the corresponding line profile (d) along the red line. Reproduced with permission from Ref. [56]. Copyright 2018, Elsevier B.V. (e) Topography of Bi nanoflakes, nanorods and nanoribbons grown on SiC buffer layer (BL) and epitaxy graphene (EG). (f) Atomic structure of Bi nanoribbon on EG. Reproduced with permission from Ref. [47]. Copyright 2018, American Chemical Society. (g) Phase diagram of the strain relief mechanism by interfacial misfit dislocations for epitaxy hetero-films. Reproduced with permission from Ref. [55]. Copyright 2020, AIP Publishing LLC.

atoms arrange and form high-quality single crystal films with controllable thickness, the surface being very smooth with roughness lower than 1 nm, even picometer level[17, 53–56]. This enables the advantage of realizing ultra-thin bismuthene with great crystallinity and high conductivity for the MBE method.

The interaction between the substrate and 2D bismuth has a crucial effect on film growth, and substrate-dependent electronic properties and orientations on various substrates are extensively studied, e.g. SiC[17], Au[56], graphene[47, 48], Si[19], Bi_2Te_3[57], and highly oriented pyrolytic graphite (HOPG)[58]. A scanning tunneling microscopy (STM) overview demonstrated the flat honeycomb monolayer bismuthene as a result of strain on insulate SiC (0001) structure in Figs. 3(a) and 3(b)[17]. The substrate temperature was controlled to ~500 °C, to condense the bismuth layer on the surface. Then post-annealing at ~400 °C was performed to improve the order of the honeycomb film. Actually, the SiC substrate forms a covalent bonding with bismuthene, generating a large topological band gap of 0.8 eV at room temperature. In contrast, the work function difference in the Au (111) substrate (5.3 eV) and Bi (4.3 eV) facilitates electron transferring from bismuthene to the Au (111) substrate, and forms Van der Waals bonding in Figs. 3(c) and 3(d)[56]. Hu *et al.* found that metallic Bi nanoflakes and nanorods prefer to epitaxy on the SiC region at low coverage stage as Fig. 3(e), but semiconducting Bi nanoribbons (bandgap of 0.5 eV) with several monolayers are formed on the epitaxial graphene (EG) region, indicating that the electronic states of Bi are substrate-dependent[47]. Fig. 3(f) shows the atomic structure of Bi (110) nanoribbon on the EG layer. Similarly, an asymmetric narrow gap (~0.4 eV) is observed in Bi nanoribbons on epitaxial graphene due to quantum and size effects and the easy electronic transfer from the substrate to Bi[48]. It is worth mentioning that (110) orientation is thermodynamically favored for epitaxial bismuthene at the initial growth stage with a thickness of several monolayers, while (111) orientation is preferred for thicker film because of the higher cohesive energy relative to (110)[59–61]. However, (111)-orientated films can also be directly prepared by altering the substrate and temperature[57, 58].

Furthermore, Meyer *et al.* reported a sudden and massive generation of misfit dislocations at a critical thickness of 4 nm in Bi (111)/Si (001) for strain relaxation in Fig. 3(g)[55]. This finding may also have implications on other epitaxial hetero-films to explore the strain state. Walker *et al.* transferred epitaxial 2D bismuth for the first time, making it realizable to measure the characteristics of bismuth films on transparent, flexible and insulating substrates[53].

Nevertheless, the MBE method has a high requirement on facility with high cost and a long experimentation period, preventing it from large-scale 2D bismuth preparation.

3.2. Pulsed laser deposition (PLD)

The PLD method uses a high energy laser to vaporize and dissociate the material under 10^{-5}–10^{-6} Pa. High ion energy promotes the adatom mobility[62], and results in smoother films than other low energy methods (evaporation or sputtering). Actually, the surface roughness of PLD 2D bismuth is several nanometers or lower than 1 nm[62–64], paving a way for fabricating smooth surface, high electrical conductivity and good crystallinity 2D bismuth.

An unusual epitaxial growth occuring on Bi/Si (100) at the beginning of the PLD process was first reported in

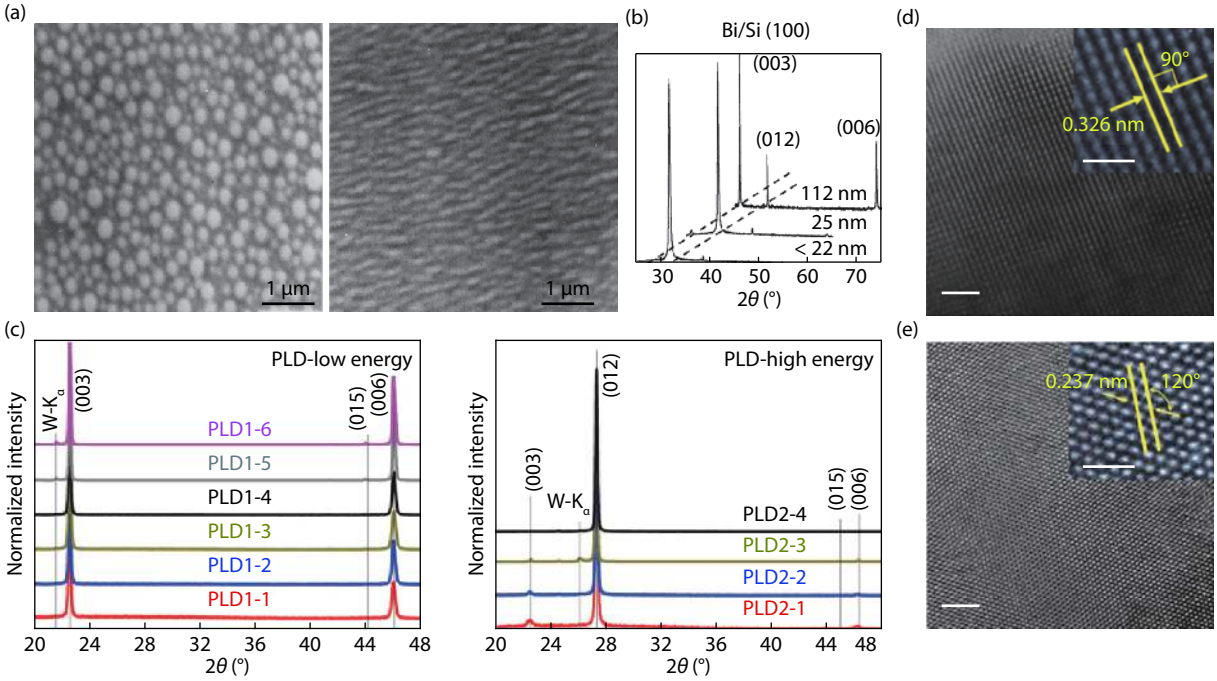

Fig. 4. (Color online) Morphology and X-ray-diffraction patterns (XRD) patterns of 2D bismuth deposited by PLD. (a) SEM micrographs of Bi films deposited by PLD at 185 °C on glass (left) and Si (100) (right). (b) Thickness-dependent XRD patterns of Bi films deposited at 20 °C on Si (100). Reproduced with permission from Ref. [63]. Copyright 1999, Elsevier Science B.V. (c) XRD patterns of the Bi thin films deposited under low ionic energy (~110 eV) and high ionic energy (~270 eV). Reproduced with permission from Ref. [62]. Copyright 2017, Elsevier B.V. (d) High-resolution TEM image of Bi (110) film and (e) Bi (111) film (scale bar = 2 nm), the inset is an enlarged image (scale bar = 1 nm). Reproduced with permission from Ref. [25]. Copyright 1999–2020, John Wiley & Sons, Inc.

1999[63]. Strong texture morphology in Fig. 4(a) and more rapid growth on Si (100) than on glass are observed by SEM and in-situ electrical resistance measurements respectively. When the thickness is less than 25 nm, the 2D bismuth deposited on the glass substrate is amorphous, while the one deposited on Si (100) has perfect crystallinity. Interestingly, in Fig. 4(b), (110) orientation is dominated below 22 nm, but transforms to (111) orientation in thicker films on Si (100). This thickness-dependent preferred orientation transforming behavior is similar to MBE prepared films as mentioned in 3.1 but with a larger critical thickness and has rarely been reported. These are explained to be epitaxial growth on Si (100) at the beginning growth regardless of misfit of 17%, which suggests that PLD could lead to something interesting that is worth studying. Note that the deposition rate is lower than 0.1 Å/pulse (or 0.5 Å/s), which may be responsible for the unusual epitaxy as the author suggested.

Substrate temperature and laser energy seriously affect the roughness, grain size and orientation of PLD 2D bismuth[25, 63, 64]. As the substrate temperature decreases, both the grain size and the film roughness are largely decreased. Hence, highly (111)-preferred orientation bismuth films are obtained at an optimized temperature of −30 °C[64].

Moreover, the low ionic energy (~110 eV) deposited samples have a pure (111) orientation in Fig. 4(c), while the high ionic energy (~270 eV) presented a (110) preferential orientation without substrate heating as Rodil reported[62]. It is claimed that low surface energy (111) planes are preferred when limiting the energy supplied to the growth process unless enough energy is supplied by substrate heating or high energy bombardment. Another study reported centimeter scale (110) and (111) oriented 2D bismuth on SiO_2/Si and Al_2O_3 substrates as shown in Figs. 4(d) and 4(e) at room temperature and 100 °C respectively. The deposition process is at a rate of ~0.2 Å/pulse[25], while Bi ion energy remaining unknown. It is obvious that the ion energy and substrate temperature of PLD have a great influence on the growth of 2D bismuth.

Compared with MBE, PLD has advantages of high deposition rates, low temperature, low cost and unlimited targets, whereas it has not demonstrated few-layer or even bilayer bismuthene yet.

3.3. Electron-beam (e-beam) evaporation

In addition to a high energy pulse laser, the electron beam can also be focused onto the surface of source material in an e-beam evaporation method. Only a small part of the source material is heated by the precisely positioned electron beam, which can minimize the evaporation of crucible materials or other possible contaminations. Precisely controlled temperature and rate allow a convenient control on thickness and properties of grown 2D bismuth.

Jankowski *et al.* reported the controllable growth of 4–20 nm 2D bismuth films with a deposition rate of ~0.02 Å/s on α-Al_2O_3(0001) insulating substrate by electron beam evaporation[65]. At temperature as low as 40 K, atomic diffusion is limited by kinetics, leading to high nucleation density of Bi island, then pseudo-cubic (110)-oriented Bi films are formed, which are stable up to 400 K. After annealing around 400 K, a competition of orientation growth between Bi (110) and Bi (111) is observed in Fig. 5(a). Above 450 K, ultra-smooth Bi (111) films are obtained directly with a lattice mismatch of 4.6% on α-Al_2O_3 (0001).

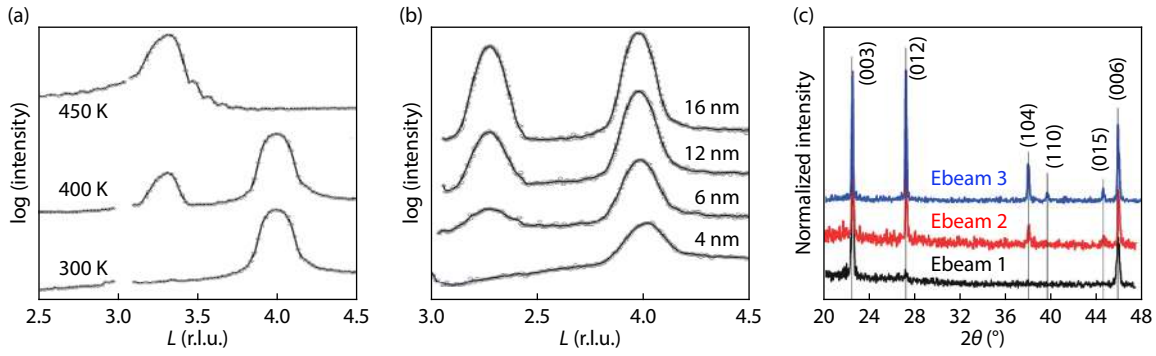

Fig. 5. (Color online) (a) X-ray reflectivity (XRR) curves for a 14 nm Bi (110) film grown at 40 K, measured at 300, 400 and 450 K. At 400 K, the onset of orientation transition towards a Bi (111) film is seen where at 450 K the entire film is transformed. (b) XRR curves for increasing Bi film thickness, grown at RT. Reproduced with permission from Ref. [65]. Copyright 2017, IOP Publishing Ltd. (c) XRD patterns of the bismuth thin films. From sample 1 to sample 3, the filament-substrate distance is decreased and film thickness increased. Reproduced with permission from Ref. [62]. Copyright 2017, Elsevier B.V.

For room temperature-deposited bismuth, Bi (110) domains are grown within the first 4 nm, followed by Bi (111) domains starting around 6 nm in Fig. 5(b)[65]. This is somewhat similar to the epitaxial 2D bismuth in which (110) is preferred at initial stage, and transform to (111) with additional thickness[59]. What they have in common is the low deposition rate which may be the precondition of commensurate growth of 2D bismuth in e-beam evaporation.

In contrast, Rodil *et al.* deposited ~180 nm Bi (111) thin films on not deliberately heated glass substrates at a high rate of ~18 Å/s by e-beam evaporation, different from low rate growth of Jankowski, and (110) orientation shows up as the thickness increases as illustrated in Fig. 5(c)[62]. It is emphasized that during the evaporation process, a low energetic deposition growth condition, atoms are usually arriving at the substrate with energy between 0.1 and 5 eV, thus less energetic Bi atoms form (111)-oriented films at low thickness, whereas the structure changed to a more random orientation as the thickness increased because the naturally increasing substrate temperature enhanced the atomic energy as indicated in Section 3.2. The bismuth thin films deposited on Si (100) by e-beam evaporation at room temperature are also consistent with this view[66].

Generally, e-beam evaporation provides a cost-effective scalable method to prepare 2D bismuth for device applications. It needs further improvements on surface roughness and precise control for few-layer bismuthene.

3.4. Thermal evaporation

In view of the low melting point of bismuth (271 °C), thermal evaporation is suitable for deposition of 2D bismuth[24, 62, 67–69]. In addition to the conventional thermal evaporation under vacuum conditions of ~10^{-4} Pa, there is also something new. Lu *et al.* prepared 2D bismuth with a thickness of 13 nm by heating Bi powder in a quartz tube furnace, which can be seen as the thermal evaporation method as in Figs. 6(a) and 6(b)[24]. At heating the temperature of 510 °C and carrier gas of N_2 under ~1 Pa, 300 nm SiO_2/Si substrates were placed 15.5–17 cm away from the heating center downstream, resulting in large-area continuous (110) orientation-dominated films. This report provides a low-cost method for the preparation of high-quality 2D bismuth. Compared to normal deposition, oblique angle deposition can reduce the size of crystallites, enhance the surface roughness and yield strongly hydrophobic bismuth thin films with a larger contact angle, which are promising in micro-channels to facilitate liquid flow for cooling in high-speed electronic devices[67]. However, undesirable large surface roughness ranging from several to tens of nanometers is a drawback for the application of CMOS which require a smooth surface.

3.5. Magnetron sputtering

The magnetron sputtering method can achieve a high deposition rate under base pressure of 10^{-4}–10^{-5} Pa, which is suitable for depositing bismuth thin films with thickness of hundreds to thousands of nanometers[62, 70, 72–74]. Under the base pressure of 8×10^{-5} Pa and the working pressure of 2.3 Pa, bismuth thin film was deposited onto the glass substrates by the magnetron sputtering method. The results showed that 160 °C is a main watershed for morphology and growth mechanism of the bismuth thin films, as shown in Fig. 6(c)[70]. Large columnar grains produced by high substrate temperature lead to an increasing value of the surface roughness as shown in Fig. 6(d) (tens to hundreds of nanometers)[62, 72, 74], not as smooth as MBE, PLD, e-beam evaporation mentioned above, thus, worse crystallinity is inevitable. For film orientation, most of the magnetron sputtered and thermal evaporated results mentioned above are consistent with Rodil's view, e.g. (111) is preferred at low temperature and (110) is preferred at elevated temperature. Similar to evaporation methods, sputtered 2D bismuth needs further optimization in terms of surface roughness for potential CMOS applications.

3.6. Flash vaporization

Flash vaporization sends fine powders bit by bit to the high temperature evaporation source where powders can realize complete evaporation in a short time. Therefore, it is easy to obtain films with the same composition as the source material.

Polycrystalline bismuth thin films with thickness of 40–160 nm was prepared via flash evaporation on preheated (453 K) glass substrates under a vacuum of 2×10^{-6} Torr for the first time[71]. Interestingly, electrical resistivity, electron concentration and mobility oscillate with increasing thickness in Figs. 6(e) and 6(f), as a consequence of the periodic step-like shape of the electron and hole density of states. Negative

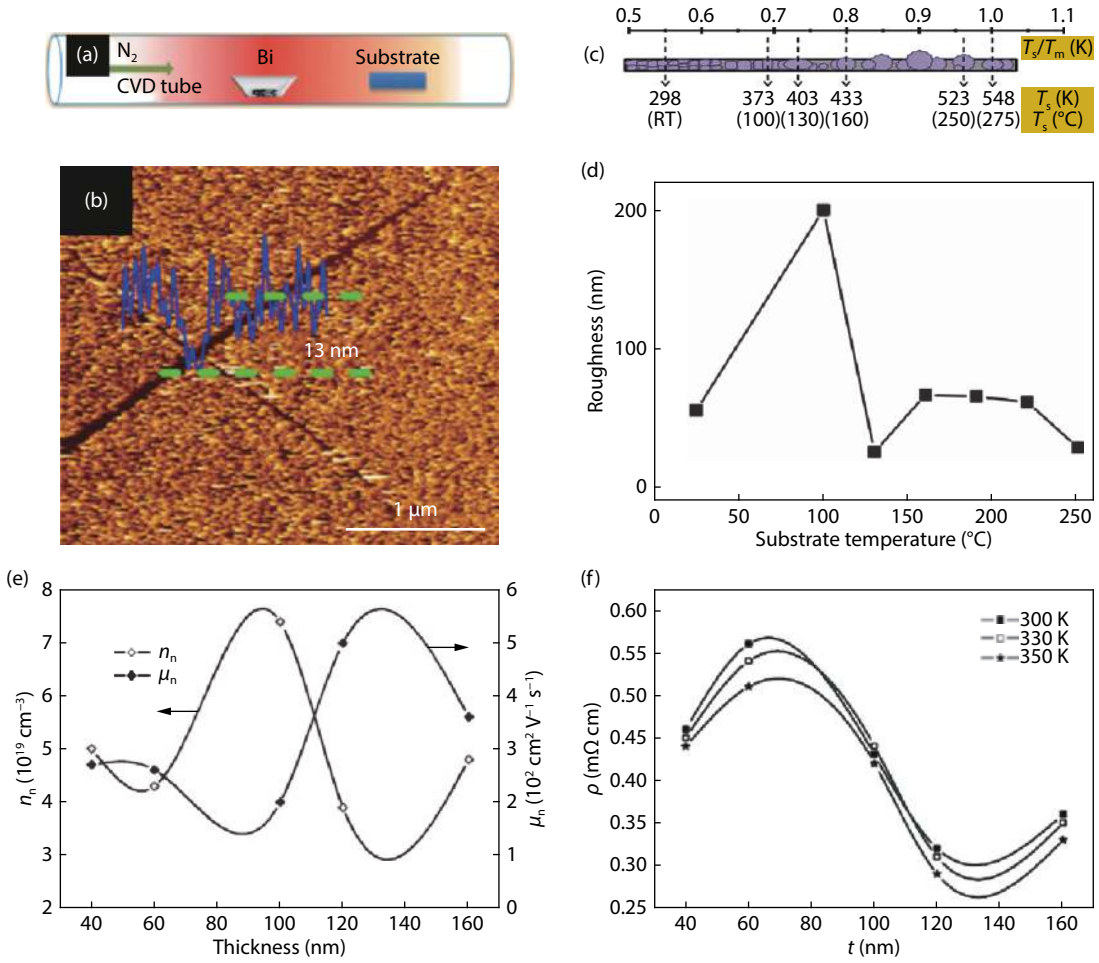

Fig. 6. (Color online) (a, b) Schematic diagram of the tube employed for the synthesis and atomic force microscopy image of 2D bismuth. Reproduced with permission from Ref. [24]. Copyright 2018, American Chemical Society. (c) Morphology evolution with substrate temperature. (d) The roughness of bismuth thin films prepared at different deposition temperatures. Reproduced with permission from Ref. [70]. Copyright 2019, Elsevier Ltd. (e) Electron concentration and mobility of flash evaporated bismuth thin films. (f) Oscillatory behavior of electrical resistivity. Reproduced with permission from Ref. [71]. Copyright 2007, Elsevier B.V.

Hall coefficients show n-type conduction. The low electrical resistivity (300 K) in the range of 0.36–0.46 mΩ cm and high electron mobility in the range of (2.7–5.0) × 10^2 cm^2 V^{-1} s^{-1} prove that high quality bismuth thin films can be prepared by flash evaporation. Recently, flash vaporization is also used in the preparation of bismuth compounds[75, 76] due to its controllable stoichiometric ratio.

Regarding the orientation of physical vapor deposited films, it can be summarized as follows: 1) for epitaxial 2D bismuth, the puckered-layered (110) phase is favored due to the higher cohesive energy for small thickness films. As thickness increasing, the situation is reversed, resulting in (111) dominated (Fig. 7). The critical thickness is 4–6 layers according to Nagao *et al.*[59, 60]. However, transition from the (110) to (111) phase can be controlled by altering the deposition temperature and substrate, making it possible to directly control the crystal orientation of 2D bismuth[42, 58, 77]. 2) For other physical vapor-deposited 2D bismuth including pulsed laser deposition, e-beam evaporation, thermal evaporation and magetronsputtering, a similar (110) to (111) transition along the increasing thickness would occur when the deposition rate is low enough[25, 63, 65]. Furthermore, at high deposition rate, there is a competitive growth of different orientation as Rodil reported: the low surface energy (111) plane is favored and the film tends to be randomly oriented or pure (110) oriented[62, 65, 66, 68, 70], unless enough energy is supplied either by substrate heating or high energy bombardment. Even so, there is still no definite conclusion about 2D bismuth orientation and (111) to (110) transition up to now, thus more research on the growth mechanism is needed.

Above-mentioned physical vapor deposition methods can realize large area continuous 2D bismuth (methods and corresponding parameters are summarized in Table 1.), which are also easy to control the size and thickness, thus, providing platforms to obtain 2D bismuth compatible with CMOS technology. Still, more attention needs to be focused on growth mechanisms since there is still a challenge to balance between low cost and high quality. In short, the MBE method has the greatest advantages in quality and controllability, while the high cost limits the possibility of large-scale preparation for CMOS applications at present. Magnetron sputtering and thermal evaporation are common methods with low cost systems, but for the deposition of ultra-thin 2D bismuth for nanoelectronic devices, the shortcomings in crystallinity and roughness are obvious. In comparison, e-beam evaporation and PLD are not as expensive as MBE, and the products are relatively smooth and high-quality films with controllable thickness, thus holding great potential for the real-

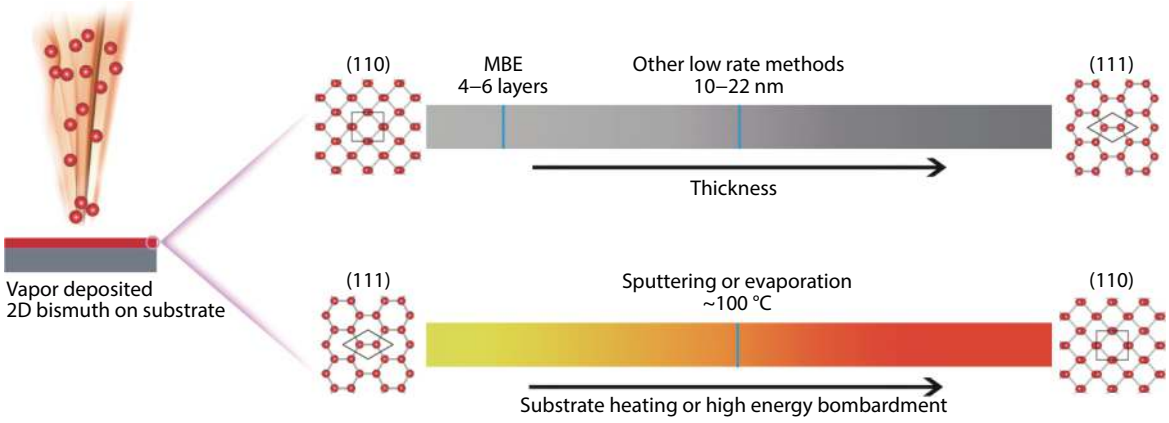

Fig. 7. (Color online) Schematic of 2D bismuth preferred orientation corresponding to different physical vapor deposition.

Table 1. Physical vapor deposition methods and corresponding parameters.

Physical vapor deposition	Pressure (Pa)	Deposition rate	Thickness	Ref.
Molecular beam epitaxy	$\sim10^{-8}$	<0.02 Å /s	1–several monolayers	[17, 56]
			~4.3–50 nm	[53–55]
Pulsed laser deposition	10^{-5}–10^{-6}	~0.1 Å/pulse	20–120 nm	[63]
		0.2–1.4 Å/pulse	1–30 nm	[25, 64]
Electron beam evaporation	10^{-4}–10^{-5}	0.02 Å/s	4–20 nm	[65]
		~18 Å/s	>100 nm	[62, 66]
Thermal evaporation	$\sim10^{-4}$	1–5 Å/s	12–100 nm	[24, 68, 69]
			>100 nm	[67]
Magnetron sputtering	10^{-4}–10^{-5}	1–5 Å/s	100–500 nm	[70, 73, 74]
			600–900 nm	[72]
Flash evaporation	$\sim10^{-4}$	–	40–160 nm	[71]

izing of large area 2D bismuth for device integration in the future.

4. 2D bismuth devices and applications

2D bismuth has been explored in a variety of CMOS relevant applications, due to good air stability and outstanding electronic properties. Below is a survey on theoretical and experimental implementations about 2D bismuth devices including field-effect transistors, sensors, photodetectors, optical devices, thermoelectric devices, topological and spintronic applications, magnetic devices and memory devices.

4.1. Field-effect transistors

A field-effect transistor is an essential building block nowadays of CMOS devices. Modern electronic chips contain billions of FETs per square millimeter[78, 79]. Although there have been tons of FET work on graphene, black phosphorus, TMDs, etc., 2D bismuth FET is still in its infancy[80]. A back-gate FET with a 10-nm-thick bismuth film channel (channel length = 30 μm, width = 500 μm) on Si wafer capped with a 300-nm-thick SiO_2 layer has been fabricated[25]. Figs. 8(a) and 8(b) show the schematic and photograph of Bi FET with 80-nm-thick Au layer as the source/drain electrodes. The output characteristics shown in Fig. 8(c) reveals a good ohmic contact between Bi and Au. The transport curve presented in Fig. 8(d) suggests a p-type channel which is Bi thin film and the field effect mobility was obtained as 220 $cm^2\ V^{-1}\ s^{-1}$, which is much larger than chemical vapor deposition (CVD) MoS_2 (3.6 $cm^2\ V^{-1}\ s^{-1}$)[81], PLD BP (10 $cm^2\ V^{-1}\ s^{-1}$)[82] and higher than silicene (100–200 $cm^2\ V^{-1}\ s^{-1}$)[83, 84]. Nonetheless, the on/off ratio of 2D bismuth FET is quite low (<10), which could be explained by the feature of semimetal. Thus, on the basis of high carrier mobility, 2D bismuth is expected to be used in high-frequency devices like BP, and showcase the potential in spintronic application.

4.2. Chemical sensors

Because of the large specific surface area and its conductance changing with the extent of surface adsorption, 2D materials are widely utilized in sensors. Several calculation works have demonstrated that 2D bismuth is a promising candidate to detect some molecules. Bhuvaneswari *et al.* reported that a bismuthene nanosheet (BiNS) was calculated to show a response to the G series which is a kind of nerve agents, revealing the application in biosensors[85]. After the adsorption of the G series, alteration in the band gap was observed, leading to change of conductivity. Princy Maria *et al.* used BiNS to detect the hazardous vapor molecules benzyl chloride and chlorobenzene by the transfer of charge, band gap and absorption energies based on the density functional theory (DFT) analysis, suggesting its prospects in chemical sensor[86]. Bismuthene nanotube was studied by Snehha *et al.* to work as a gas sensor material for trace amounts of NH_3, NO_2 and PH_3, using the Perdew–Burke–Ernzerhof (PBE) function[87]. Although theoretical research has been carried out intensively, there is a lack of experimental reports on 2D bismuth based sensor. Since the excellent sensing behavior predicted by DFT and PBE analysis, 2D bismuth chemi-resistor sensors will emerge in the next few years.

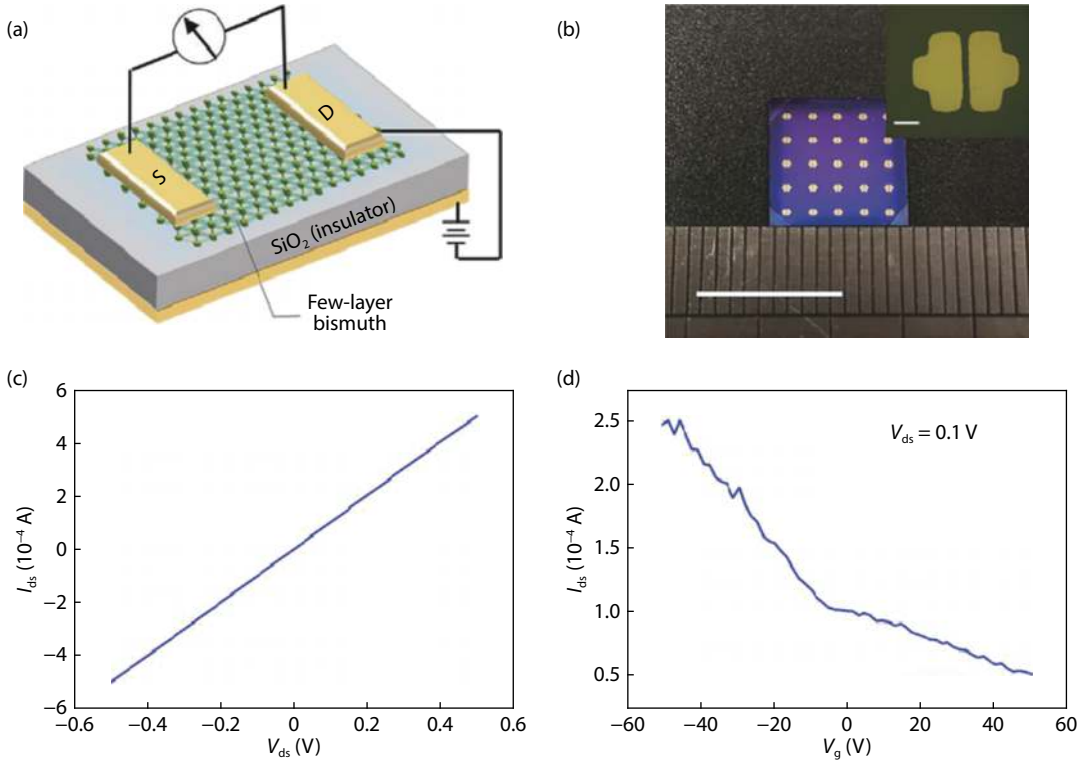

Fig. 8. (Color online) Transport properties characterization of PLD grown Bi (111) films. Reproduced with permission from Ref. [25]. Copyright 1999–2020, John Wiley & Sons, Inc. (a) The schematic of FETs based on Bi film. (b) Photograph of Bi FETs with patterned Au electrode (scale bar = 1 cm). The inset shows the optical picture of the electrode pattern of the device (scale bar = 100 μm). (c) Drain current-voltage output characteristics with gate bias at 0 V and (d) Drain current-gate voltage curve of the FET based on 10-nm-thick Bi film.

4.3. Photodetectors and optical devices

Bi is favored for ultra-broadband and high-responsive photodetectors due to its metallic surface state and small bulk gap. Yao *et al.* used PLD-grown Bi thin film to prepare a photodetector shown in Fig. 9(a)[88]. An obvious switching behavior (Fig. 9(b)) was observed with a rather prompt response (0.9 s) and decay time (1.9 s). A high responsibility (c.a. 250 mA/W) was extracted[88], which is much larger than graphene and MoS_2. Nonetheless, the calculated photosensitivity is quite low (0.02 cm^2/W). Fig. 9(c) reveals that the Bi-photodetector presents an ultra-broadband range response from ultraviolet (370 nm) to infrared (1550 nm) [88]. The mechanism of the Bi photodetector was shown in Fig. 9(d). The laser leads to the generation of electron–hole pairs and then move to the electrodes under the action of an external electric field to a photocurrent. Besides, a high-performance self-powered flexible photodetector based on CVD-Bi/polyimide (see Fig. 9(e)) was fabricated by Zhou *et al.*[89]. It has not only fast rise and decay time but also durability and reproducibility after bending various radii of curvature and over 100 folding cycles. The time-dependent photocurrent was presented in Fig. 9(f).

Bismuthene was proved to be applied in nonlinear optical applications. Lu *et al.* characterized its nonlinear optical response at the visible band by Z-scan and cross-phase modulation (XPM) methods[90]. They utilized the XPM effect in bismuthene to achieve all optical switching in spatial domain. Figs. 10(a)–10(c) shows the formation process of 532 nm laser of all-optical switching based on XPM, the changes of switching light leading to that of rings of signal light. Fig. 10(d) is the schematic experimental setup of XPM[90]. In addition to optical switch, Chai *et al.* demonstrated a dissipative soliton ytterbium-doped mode-locked fiber laser at 1 μm regime with a bismuthene saturable absorber (SA) by using evanescent field interaction for the first time[91]. The nonlinear transmittance of the SA (Fig. 10(e)) indicates saturation intensity and modulation depth are about 13 MW/cm^2 and 2.2%[91]. A robust ultrafast pulse generation in the communications-band based on few-layer bismuthene has also been reported[94]. Nevertheless, the bismuthene above is prepared by sonochemical exfoliation, while optical properties of physical vapor deposited 2D bismuth have rarely been investigated.

4.4. Thermoelectric devices

As a post-transition metal with a carrier mobility of up to ~ 20 000 $cm^2\,V^{-1}\,s^{-1}$[26], bismuth has the lowest metal thermal conductivity except mercury of 10 W m^{-1} K^{-1}[95, 96]. Given the mean free path of phonons is longer than electrons, the properties of bismuth are very conducive to the thermoelectric performance that can convert heat into electricity. The efficiency of conversion is determined by the dimensionless figure of merit (zT), as $zT = \frac{S^2\sigma}{\kappa}T$, where S stands for the Seebeck coefficient, σ denotes the electrical conductivity, κ represents the thermal conductivity and T is the temperature. It is worth noting that there is a gap in the thermoelectric performance of bismuth, compared with commercial thermoelectric materials like Bi_2Te_3, due to the much smaller Seebeck coefficient[97–100].

Fortunately, according to the quantum confinement effect of Hicks & Dresselhaus[92, 101, 102], bismuthene with reduced thickness would overturn this situation in terms of min-

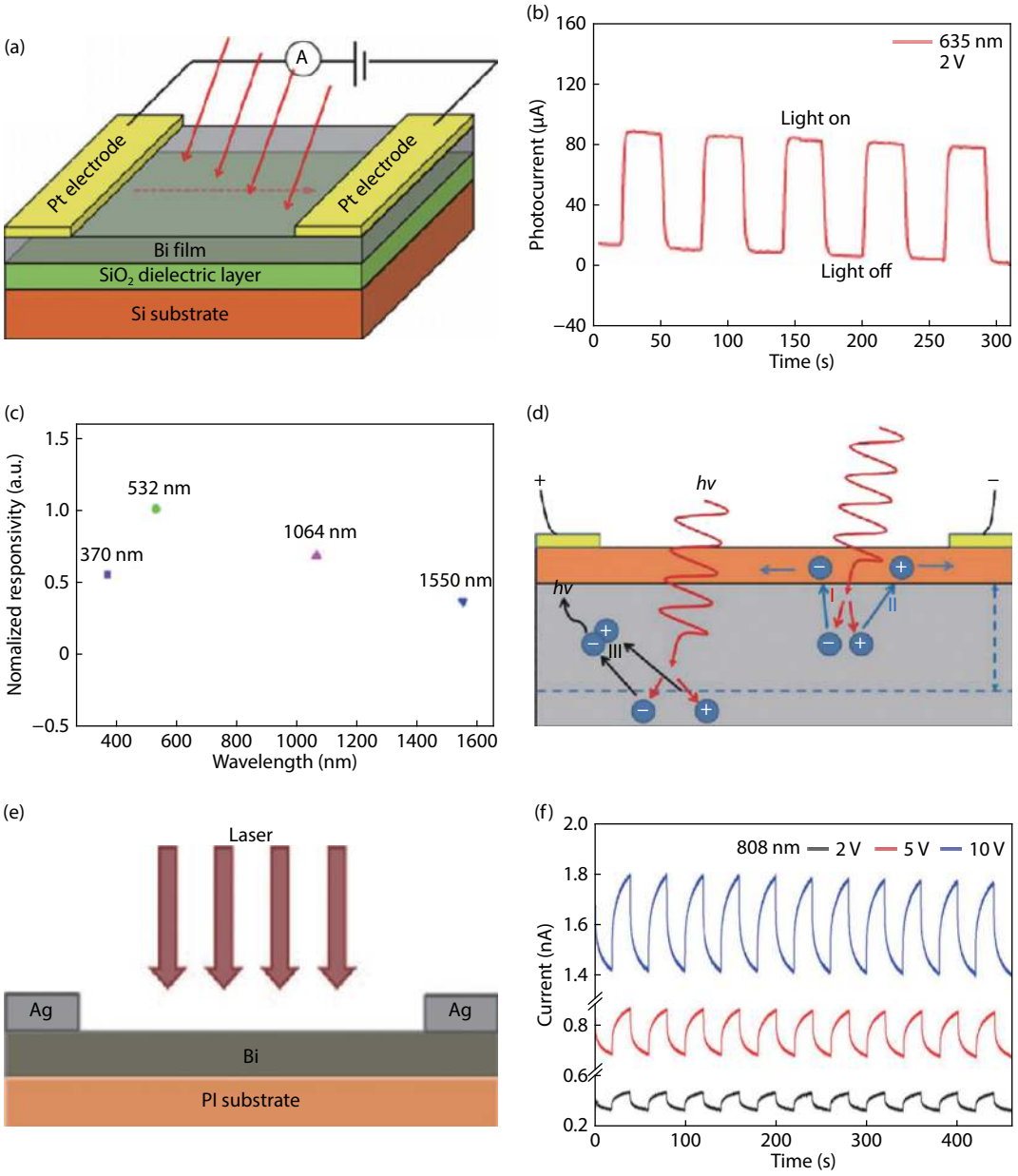

Fig. 9. (Color online) (a) Three-dimensional schematic view of the Bi photodetector. (b) Time-dependent switching behavior of the photocurrent. Device area: 0.32 × 0.32 mm^2. Power density: 300 mW/cm^2. (c) Normalized responsivity as a function of illumination wavelength. Device size: 2 × 1.2 mm^2. (d) Operating mechanism of the Bi photodetector. Reproduced with permission from Ref. [88]. Copyright 2015, Springer Nature. (e) Schematic view of the flexible Bi photodetector on the PI substrate. (f) Time-dependent photocurrent in the flexible photodetector excited by 808 nm laser with bias voltages of 2, 5, and 10 V. Reproduced with permission from Ref. [89]. Copyright 2020, American Chemical Society.

imizing thermal conductivity while increasing the Seebeck-coefficient and keeping high electrical conductivity. For bismuth, it is predicted to show the quantum confinement effect below ~30 nm (Fig. 10(f)). As the thickness of the film is further reduced to less than 1 nm, zT value of bismuthene can exceed to 8 (zT up to 1 is expected for commercial use). Based on the quantum confinement effect, some researchers have focused on the thermoelectric properties of bismuthene theoretically in recent years. Wu *et al.*[103] used the first-principles and Boltzmann transport theory to calculate the Seebeck coefficient of the single-layer bismuthene (~ 342 μV/K). In another calculation, the Seebeck coefficient of single-layer bismuthene can reach up to ~ 320 μV/K and the zT value can be 2.4 at room temperature[93] (Fig. 10(g)). These theoretical predictions supported the above theories and indicated that reducing the thickness of 2D bismuth to a certain extent could improve the Seebeck coefficient, making it an ideal material for applications in thermoelectric devices. But in fact, due to the potential influence of surface charge and substrate coupling effect, the actual critical thickness may deviate from the theoretical value according to quantum confinement effect.

Recently, Yang *et al.*[25] used pulsed laser deposition to grow 2D bismuth with the thickness of less than 30 nm on the SiO_2 substrate, but they did not report the thermoelectric properties of the bismuth film. Xu *et al.*[104] theoretically discussed the thermoelectric properties of topological insulators (TIs) materials and showed that the thermoelectric properties of TIs depend on the geometric size, which provides a new idea for improving the zT values of TIs like bis-

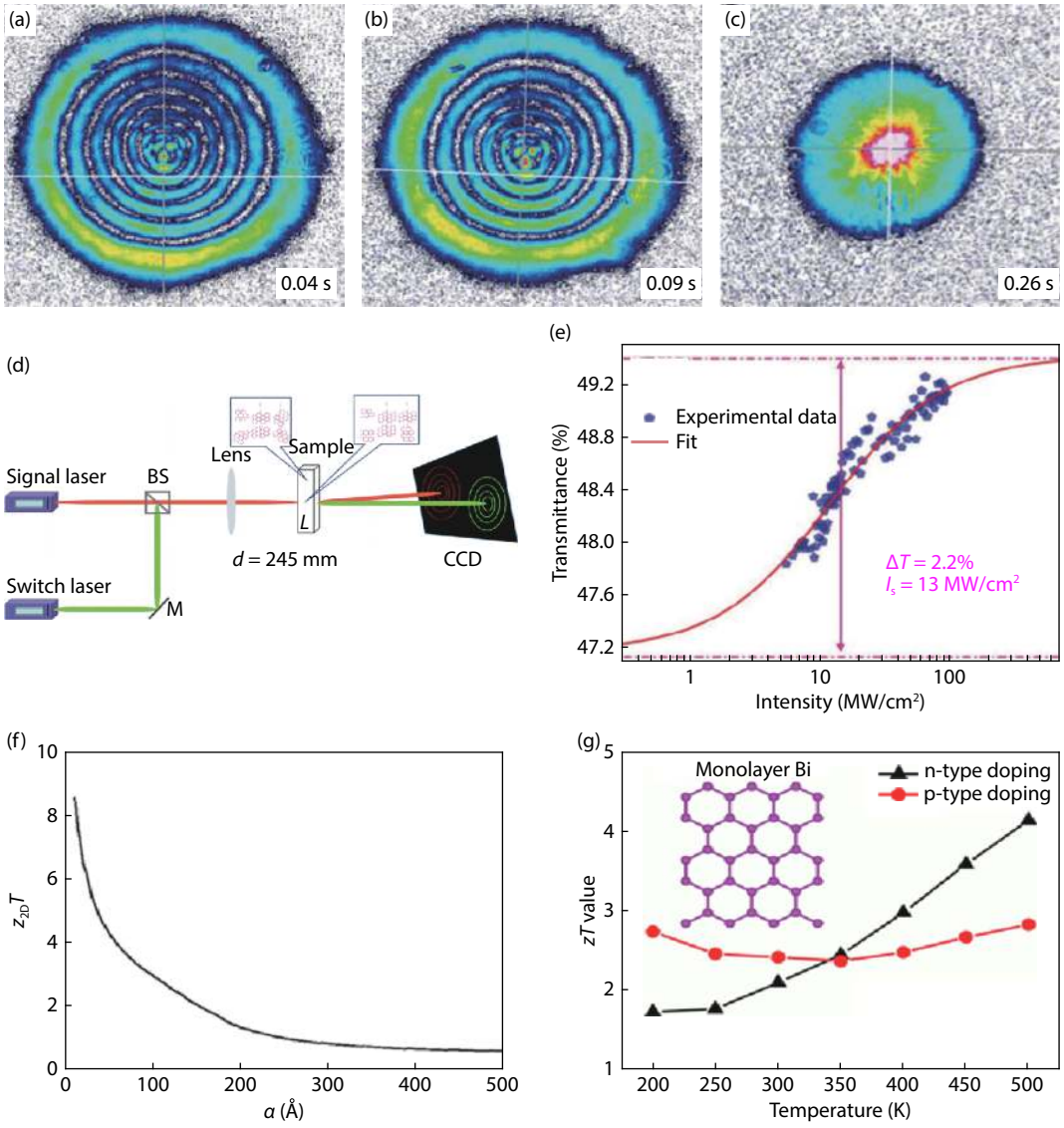

Fig. 10. (Color online) (a–c) Formation process of all-optical switching based on XPM using 532 nm laser with intensity at 5.48 W/cm^2. (d) Schematic experimental setup of XPM. Reproduced with permission from Ref. [90]. Copyright 2017, American Chemical Society. (e) Nonlinear transmittance and fitting curve. Reproduced with permission from Ref. [91]. Copyright 2018, The Royal Society of Chemistry. (f) Predicted zT value of bismuth thin films with different quantum wells. Reproduced with permission from Ref. [92]. Copyright 2020, AIP Publishing LLC. (g) Predicted zT value of monolayer bismuthene. Reproduced with permission from Ref. [93]. Copyright 2020, American Chemical Society.

muthene. Actually, as early as the 1990s, Das *et al.*[105] and Cho *et al.* [106] measured the Seebeck coefficient of bismuth thin films at room temperature (~ 60 μV/K). However, experimental results of thermoelectric properties, such as zT values of 2D bismuth are still lacking. So far, no one has reported the zT value of the 2D bismuth below 30 nm.

There are still great challenges and prospects for further research on the thermoelectric properties of 2D bismuth in the future, such as avoiding the oxidation during growth, controlling the surface roughness of thin films and unifying the instrument standard for the thermoelectric measurement of 2D materials.

4.5. Topological and spintronic device

Koroteev *et al.* found strong spin-orbit splitting on Bi surfaces[16], suggesting the spintronic applications of 2D bismuth. Bi has high magnetic susceptibility, resistivity, Hall coefficient and low heat conductivity. Thus, 2D bismuth became a candidate for the topological insulator (TI). Bi (111) is a honeycomb-like hexagonal lattice, so its surface electronic state has the energy band structure of a multi-energy valley with a vortex-like spin state[107]. Combining first-principles calculations and STM/STS experimental studies, Lu *et al.* reported the nontrivial 2D TI phases in 2-monolayer (2-ML) and 4-ML Bi (110) films with large and tunable bandgaps determined by atomic buckling of Bi (110) films. Their topological property is sensitive to atomic buckling which is sensitive to charge doping and could be controlled by different substrates[36]. Du *et al.* reported the determination of surface-state Landau levels (see Fig. 11(a)) in deposited Bi (111) film under different magnetic fields via STM and the identification of some specific surface spin states with a large g-factor[107]. Their findings throw light on the applications of 2D bismuth in topological devices and spintronics.

Quantum spin Hall (QSH) material has edge conductance channels, which can prevent some types of scattering, and is a hope for a revolutionary device without loss of spin

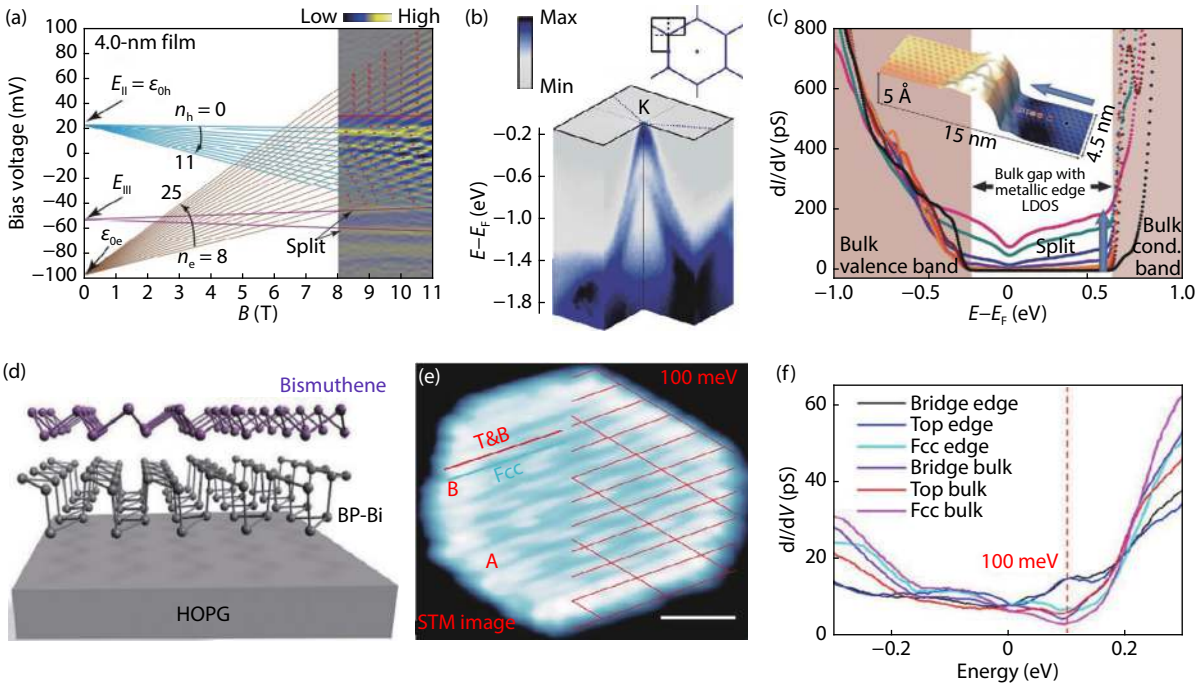

Fig. 11. (Color online) (a) The second derivative of the Landau-level (SDLL) pattern of the 4.0-nm-thick film as a function of B. Acquisition conditions: −150 mV and 4 nA, modulation of 1.0 mV by root mean square. Reproduced with permission from Ref. [107]. Copyright 2016, Springer Nature. (b) Close-up of ARPES showing a valence-band maximum at the K point with large SOC-induced splitting in a wide momentum range. The sketch in the top-right corner depicts the orientation of the cut (black lines) in the momentum space of the SBZ (blue hexagon). (c) Differential conductivity d*I*/d*V* (reflecting the LDOS) at different distances to the edge. Reproduced with permission from Ref. [17]. Copyright 2020, American Association for the Advancement of Science. (d) Illustration of bismuthene/BP-Bi vertical homostructure on HOPG substrate. (e) STM image of a typical bismuthene island on BP-Bi layer. The red grid is superimposed in the right half of the bismuthene island to highlight the moiré superlattice. Scale bars, 40 Å. (f) d*I*/d*V* curves taken at three inequivalent sites at the edge and the center part of bismuthene island, respectively (set point: V_s = 0.3 V, I = 500 pA). Reproduced with permission from Ref. [108]. Copyright 2020, American Association for the Advancement of Science.

current[17]. Reis *et al.* fabricated bismuthene on SiC (0001) via MBE (as shown in Fig. 3(b)) for TI investigation[17]. Bismuthene was detected to have a conductive edge state consistent with theory. They used ARPES to test the topological boundary states, deriving a large band splitting of ~0.43 eV (Fig. 11(b)). And the STS result shown in Fig. 11(c) reveals the existence of bismuthene edges at SiC-substrate steps and a large bulk gap of ~800 meV[17]. Besides, it is exciting that Gou *et al.* reported the successful growth of a bismuth homostructure[108] consisting of monolayer bismuthene and single-layer black phosphorus-like Bi on the HOPG surface as shown in Fig. 11(d). The formation of moiré superstructures (Fig. 11(e)) improves the decoupling between layers, preserving the topological properties of monolayer bismuthene. On the other hand, it also brings the modulation of topological edge states of bismuthene (Fig. 11(f)). Their work suggests a promising method to tailor the topological states by interfacial interactions.

It is inspiring to apply 2D bismuth to spintronic and topological devices, which can reduce power consumption and increase the running speed of CMOS.

4.6. Magnetoresistance and memory applications

High-performance magnetic and current sensors are widely used in integrated circuits and magnetoresistance (MR) materials are promising in this field. The giant magnetoresistance (GMR) head is more sensitive than the MR head. In other words, the same magnetic field change can cause a greater resistance value change for GMR head. It can achieve a higher storage density, holding a great prospect in CMOS. The following work reveals the giant magnetoresistance property of 2D bismuth and its potential applications in resistive memories.

Yang *et al.* fabricated 1–20 μm thick single crystal bismuth thin film by electrodeposition and suitable annealing and observed the MR up to 250% at 300 K and 380 000% at 5 K[109], buried for the giant magnetoresistance of 2D bismuth. Wang *et al.* characterized that MR of MBE prepared polycrystalline 29–193 nm thick bismuth thin film was ~25% at 230 K and ~325% at 125 K in 9 T magnetic field[110], respectively (see Figs. 12(a) and 12(b)). It is attributed to the compensation of electron and hole when the magnetic field is applied at the electron–hole resonance. Wang *et al.*[111] investigated the temperature dependence of R&MR and magnetic field dependence of MR of MBE-Bi film with different sample tilt angle θ at 300 K (see Figs. 12(c) and 12(d)). The MR reached ~320% at ~130 K, demonstrating that low-cost polycrystalline Bi film can achieve large MR.

Xu *et al.* reported the reversible and nonvolatile tuning of electronic transport properties of the Bi-based heterostructures[112]. Bismuth thin film (85 nm) was grown on (111)-oriented 0.7Pb($Mg_{1/3}Nb_{2/3}$)O_3–0.3$PbTiO_3$ (PMN–PT) single-crystal substrates by PLD. Non-volatile resistance modulation and multiple resistance state can be achieved by polarization switching, appropriate electric fields applying and magnetic

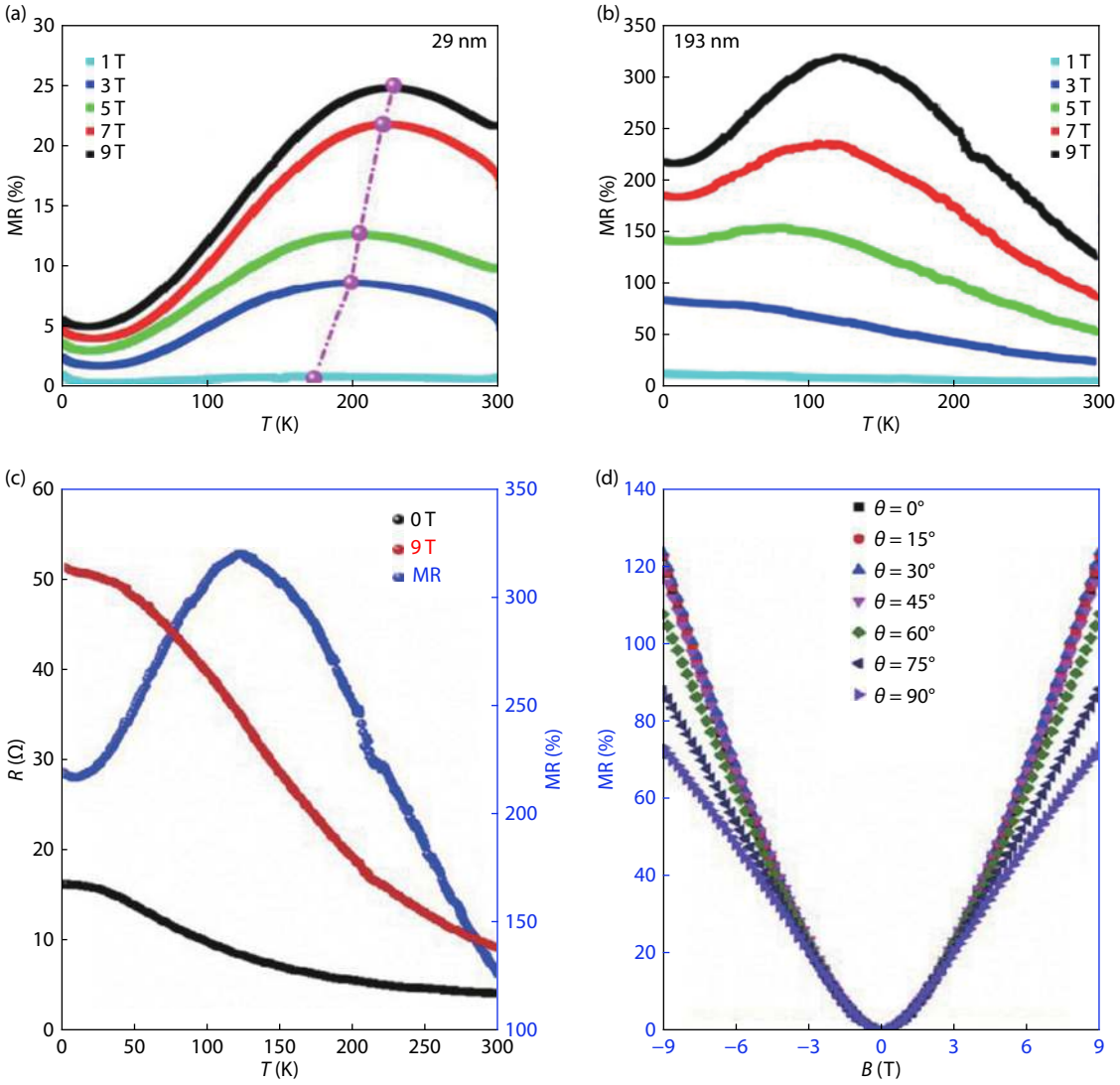

Fig. 12. (Color online) (a, b) Calculated temperature dependence of the magnetoresistance ratio for 29 nm and 193 nm bismuth thin films. Reproduced with permission from Ref. [110]. Copyright 2020, AIP Publishing LLC. (c) The temperature dependence of R and MR of bismuth thin film with thickness of 200 nm in 0 and 9 T, and (d) the magnetic field dependence of MR of bismuth thin film with different sample tilt angle θ at 300 K. Reproduced with permission from Ref. [111]. Copyright 2019, Elsevier Ltd.

field controlling.

To sum up, 2D bismuth has been studied in many aspects of the CMOS field including high mobility FET, ultrabroadband and high-responsive photodetectors, optical, thermoelectric and topological devices. But there is a lack of experimental study on sensors and spintronic devices, urgently needing further research. Besides, the giant magnetoresistance of bismuth will become a fascinating application in the near future. It can be optimistically predicted that 2D bismuth will hold a bright prospect in CMOS.

5. 2D bismuth derivatives (Bi–X)

Even though 2D bismuth has many peculiar properties, there will still be limitations for an elemental 2D material to realize various applications. Many strategies can be performed to enrich the properties and applications of 2D bismuth including doping, defect, strain, alloying and so on. The alloying method can be viewed as doping new atoms into Bi crystal[4, 113, 114], such as $Bi_{1-x}Sb_x$, Bi_2Te_3 and Bi_2Se_3.

Bi and Sb share the same rhombohedral structure, so they could form a continuous solid solution, namely $Bi_{1-x}Sb_x$. Bulk $Bi_{1-x}Sb_x$ is a small gap topological insulator (bandgap < 20 meV) when $0.07 < x < 0.22$ whereas a semimetal when $x < 0.07$ or $x > 0.22$[115, 116]. This composition dependent bandgap will bring a new degree of freedom to adjust properties. Actually, a band gap of 35 meV at $x = 0.15$ for 90 nm $Bi_{1-x}Sb_x$ films[115] has been reported by Ueda *et al.* The conductivity of 2D $Bi_{1-x}Sb_x$ exceeds 10^5 Ω^{-1} m^{-1} which is higher than that of 2D bismuth. And the metallic surface states demonstrate the potential of $Bi_{1-x}Sb_x$ as a spin Hall material with high electrical conductivity and possibly large spin Hall angle for spintronic applications. Additionally, semiconducting Bi-rich 2D $Bi_{1-x}Sb_x$ is a promising thermoelectric material at low temperature[116–118]. The substitution of Bi by Sb atom in β-BiSb monolayer will decrease phonon group velocities and phonon lifetimes, which fundamentally leads to the decreased lattice thermal conductivity (0.55 W m^{-1} K^{-1}) than that of β-Bismuthene monolayer (1.23 W m^{-1} K^{-1})[40, 119] and an improved zT value (0.82 and 0.77 for electrons and holes, respectively).

Bismuth telluride (Bi_2Te_3) or bismuth selenide (Bi_2Se_3)

have attracted immense interest due to their exceptional thermoelectric and optoelectronic properties. Bi_2Te_3 and Bi_2Se_3 also possess the rhombohedral crystal structure with the space group $D^5_{3d}(R\bar{3}m)$. Both crystals can be disassemble into quintuple building blocks, consisting of Te(Se)$^{(1)}$–Bi–Te(Se)$^{(2)}$–Bi–Te(Se)$^{(1)}$. The intralayer atoms are tightly bounded by covalent bonds, but the interlayer coupling are weak due to the existence of the Van der Waals gap[120].

In bulk form, Bi_2Te_3 and Bi_2Se_3 single crystal have more excellent thermoelectric performance compared with Bi. Here, we mainly focus on the figure of merit *zT*, which is a critical parameter to characterize the performance of thermoelectric materials. Researchers have founded that the *zT* values of bulk Bi_2Se_3 and Bi_2Te_3 are 0.11[121] and 0.26[122], respectively, significantly higher than that of bulk bismuth at 0.059[96]. Cheng *et al.* obtained the *zT* value of single-layer Bi through theoretical calculation. The maximum *zT* value of n-type single-layer Bi is 2.1, and the maximum *zT* value of p-type single-layer Bi is 2.4[93]. In comparison, single-layer Bi_2Te_3 and Bi_2Se_3 have higher *zT* values caused by quantum confinement effect. Zahid *et al.*[123] have reported the *zT* value of single-layer Bi_2Te_3 was 7.15 at 300 K. Guo *et al.* have reported the maximal *zT* value of single-layer Bi_2Se_3 is 19 at 900 K when the carrier concentration is fixed at 3.24×10^{18} cm^{-3}. Taking the anisotropy into consideration, the highest *zT* = 25 was obtained along the *xx* direction[124].

Furthermore, Bi_2Te_3 and Bi_2Se_3 are expected to be important photoelectric materials for high-performance terahertz to infrared applications, due to the small bandgap, thickness and size-dependent light absorption, and tunable surface bandgap characteristics[125, 126]. We compared responsivity (*R*) and response time (τ) of photodetectors based on Bi, Bi_2Te_3 and Bi_2Se_3, respectively. The photodetector performance of Bi_2Te_3 flakes stripped by using the scotch tape method (R = 74.32 A/W, τ_{rising}= 0.42 s and τ_{decay}= 0.44 s)[125] and Bi_2Se_3 flakes via van der Waals epitaxy (R = 2.74 A/W, τ_{rising}= 0.54 s and τ_{decay}= 0.47 s)[126] are much better than that of PLD-grown Bi films ($R = 250 \times 10^{-3}$ A/W, τ_{rising}= 0.9 s and τ_{decay}= 1.9 s)[88].

Bismuth derivatives indicate that composite element is an effective method to tune the properties for more versatile device performance.

6. Summary and perspectives

In this review, CMOS technology compatible physical vapor deposition methods of 2D bismuth are summarized especially focusing on epitaxy, evaporation and sputtering as well as preferred orientation of vapor deposited films. This sort of method provides a platform for synthesizing 2D bismuth with more flexible and controllable capability. Benefiting from fascinating electrical and thermal properties, 2D bismuth has a great potential in next-generation nanodevices according to experimental and theoretical investigations, which can be applied to CMOS such as transistors, sensors, optical modulators, spintronic and memory devices. In addition, an alloying strategy (Bi–X, X = Sb, Te, Se) is mentioned for further enhanced performance. Emerging 2D Xene, like bismuthene in this review, has drawn tremendous attention in CMOS related nanodevices. With atomic precision in layer control and scalability, physical vapor deposition techniques have advantages in realization of large-area, uniform and high-quality 2D bismuth for future CMOS compatible technology.

Despite the rapid development and promising achievements of 2D bismuth in recent years, there are remaining challenges for experimental study and practical applications. First, a low-cost and high-quality deposition method should be testified for industrial production of wafer-scale 2D bismuth. The recognized high-quality molecular beam epitaxy method, is costly and time consuming, making it limited to laboratory research. Traditional evaporation or sputtering methods need to be improved to yield smoother films with better quality for CMOS devices. Many potential applications are still in the stage of theoretical simulations. In-depth experimental research on material properties and device integration are necessary to narrow the gap between theoretical and experimental research on 2D bismuth. Moreover, advanced characterization techniques for 2D materials should be developed to obtain more precise results about the growth mechanism, properties and device performance. Nano scale device integration techniques also need improvement to accommodate the smaller size and higher integration density in the CMOS technique. Rational design and modification approaches such as alloying, doping, external magnetic field or strain, play an important role in determining electronic, chemical and physical properties of 2D bismuth, which can further enhance the performance and give birth to novel device applications.

Acknowledgements

This work was supported by the National Natural Science Foundation of China (No. 51602051), Jiangsu Province Innovation Talent Program, Jiangsu Province Six-Category Talent Program (No. DZXX-011).

References

[1] Zhang S, Xie M, Li F, et al. Semiconducting group 15 monolayers: A broad range of band gaps and high carrier mobilities. Angew Chem Int Ed, 2016, 55(5), 1666

[2] Zhu Z, Tománek D. Semiconducting layered blue phosphorus: A computational study. Phys Rev Lett, 2014, 112(17), 176802

[3] Zhang J L, Zhao S, Han C, et al. Epitaxial growth of single layer blue phosphorus: A new phase of two-dimensional phosphorus. Nano Lett, 2016, 16(8), 4903

[4] Zhang S, Guo S, Chen Z, et al. Recent progress in 2D group-VA semiconductors: from theory to experiment. Chem Soc Rev, 2018, 47(3), 982

[5] Tran V, Soklaski R, Liang Y F, et al. Layer-controlled band gap and anisotropic excitons in few-layer black phosphorus. Phys Rev B, 2014, 89(23), 235319

[6] Qiao J, Kong X, Hu Z X, et al. High-mobility transport anisotropy and linear dichroism in few-layer black phosphorus. Nat Commun, 2014, 5, 4475

[7] Li L, Yu Y, Ye G J, et al. Black phosphorus field-effect transistors. Nat Nanotechnol, 2014, 9(5), 372

[8] Beladi-Mousavi S M, Pumera M. 2D-pnictogens: alloy-based anode battery materials with ultrahigh cycling stability. Chem Soc Rev, 2018, 47(18), 6964

[9] Kim J S, Liu Y, Zhu W, et al. Toward air-stable multilayer phosphorene thin-films and transistors. Sci Rep, 2015, 5, 8989

[10] Pizzi G, Gibertini M, Dib E, et al. Performance of arsenene and antimonene double-gate MOSFETs from first principles. Nat Commun, 2016, 7, 12585

[11] Chia H L, Latiff N M, Gusmao R, et al. Cytotoxicity of shear exfoliated pnictogen (As, Sb, Bi) nanosheets. Chemistry, 2019, 25(9), 2242
[12] Zhang S, Yan Z, Li Y, et al. Atomically thin arsenene and antimonene: Semimetal–semiconductor and indirect–direct band-gap transitions. Angew Chem Int Ed, 2015, 54(10), 3112
[13] Ares P, Aguilar-Galindo F, Rodríguez-San-Miguel D, et al. Mechanical isolation of highly stable antimonene under ambient conditions. Adv Mater, 2016, 28(30), 6332
[14] Gusmao R, Sofer Z, Bousa D, et al. Pnictogen (As, Sb, Bi) nanosheets for electrochemical applications are produced by shear exfoliation using kitchen blenders. Angew Chem Int Ed, 2017, 56(46), 14417
[15] Kim S H, Jin K H, Park J, et al. Topological phase transition and quantum spin Hall edge states of antimony few layers. Sci Rep, 2016, 6(1), 33193
[16] Koroteev Y M, Bihlmayer G, Gayone J E, et al. Strong spin-orbit splitting on bi surfaces. Phys Rev Lett, 2004, 93(4), 046403
[17] Reis F, Li G, Dudy L, et al. Bismuthene on a SiC substrate: A candidate for a high-temperature quantum spin Hall material. Science, 2017, 357(6384), 287
[18] Hirahara T, Nagao T, Matsuda I, et al. Quantum well states in ultrathin Bi films: Angle-resolved photoemission spectroscopy and first-principles calculations study. Phys Rev B, 2007, 75(3), 035422
[19] Hirahara T, Nagao T, Matsuda I, et al. Role of spin-orbit coupling and hybridization effects in the electronic structure of ultrathin Bi films. Phys Rev Lett, 2006, 97(14), 146803
[20] Hofmann P. The surfaces of bismuth: Structural and electronic properties. Prog Surf Sci, 2006, 81(5), 191
[21] Sun J T, Huang H, Wong S L, et al. Energy-gap opening in a Bi110 nanoribbon induced by edge reconstruction. Phys Rev Lett, 2012, 109(24), 246804
[22] Hoffman C A, Meyer J R, Bartoli F J, et al. Semimetal-to-semiconductor transition in bismuth thin films. Phys Rev B, 1993, 48(15), 11431
[23] Ast C R, Hochst H. Fermi surface of Bi(111) measured by photoemission spectroscopy. Phys Rev Lett, 2001, 87(17), 177602
[24] Lu D L, Luo S W, Liu S H, et al. Anomalous temperature-dependent Raman scattering of vapordeposited two-dimensional Bi thin films. J Phys Chem C, 2018, 122, 24459
[25] Yang Z, Wu Z, Lyu Y, et al. Centimeter-scale growth of two-dimensional layered high-mobility bismuth films by pulsed laser deposition. Info Mat, 2019, 1, 98
[26] Partin D L, Heremans J, Morelli D T, et al. Growth and characterization of epitaxial bismuth films. Phys Rev B, 1988, 38(6), 3818
[27] Liu Y, Allen R E. Electronic structure of the semimetals Bi and Sb. Phys Rev B, 1995, 52(3), 1566
[28] Li L, Tang C, Xia B, et al. Two-dimensional mosaic bismuth nanosheets for highly selective ambient electrocatalytic nitrogen reduction. ACS Catal, 2019, 9(4), 2902
[29] Huang Y, Zhu C, Zhang S, et al. Ultrathin bismuth nanosheets for stable Na-Ion batteries: Clarification of structure and phase transition by in situ observation. Nano Lett, 2019, 19(2), 1118
[30] Hao C, Wen F, Xiang J. Liquid-exfoliated black phosphorous nanosheet thin films for flexible resistive random access memory applications. Adv Funct Mater, 2016, 26(12), 2016
[31] Xu Y, Yuan J, Zhang K. Field-induced n-doping of black phosphorus for CMOS compatible 2D logic electronics with high electron mobility. Adv Funct Mater, 2017, 27(38), 1702211
[32] Radisavljevic B, Radenovic A, Brivio J. Single-layer MoS_2 transistors. Nat Nanotechnol, 2011, 6(3), 147
[33] Schwierz F. Graphene transistors. Nat Nanotechnol, 2010, 5(7), 487
[34] Norman N C. Chemistry of arsenic, antimony and bismuth. Springer Science & Business Media, 1997
[35] Wada M, Murakami S, Freimuth F, et al. Localized edge states in twodimensional topological insulators: ultrathin Bi films. Phys Rev B, 2011, 83(12), 121310
[36] Lu Y, Xu W, Zeng M, et al. Topological properties determined by atomic buckling in self-assembled ultrathin Bi (110). Nano Lett, 2015, 15(1), 80
[37] Liu Z, Liu C X, Wu Y S, et al. Stable nontrivial Z2 topology in ultrathin Bi (111) films: a first principles study. Phys Rev Lett, 2011, 107(13), 136805
[38] Wu C Y, Han J C, Sun L, et al. Effects of trigonal deformation on electronic structure and thermoelectric properties of bismuth. J Phys: Condens Matter, 2018, 30(28), 285504
[39] Guo Y, Pan F, Ye M, et al. Monolayer bismuthene–metal contacts: A theoretical study. ACS Appl Mater Interfaces, 2017, 9(27), 23128
[40] Wu C Y, Sun L, Han J C, et al. Effects of low dimensionality on electronic structure and thermoelectric properties of bismuth. RSC Adv, 2019, 9(69), 40670
[41] Yaginuma S, Nagao T, Sadowski J T, et al. Origin of flat morphology and high crystallinity of ultrathin bismuth films. Surf Sci, 2007, 601(17), 3593
[42] Liu X, Zhang S, Guo S, et al. Advances of 2D bismuth in energy sciences. Chem Soc Rev, 2020, 49(1), 263
[43] Akturk E, Uzengi Akturk O, Ciraci S. Single and bilayer bismuthene: Stability at high temperature and mechanical and electronic properties. Phys Rev B, 2016, 94(1), 014115
[44] Lee J, Tian W C, Wang W L, et al. Two-dimensional pnictogen honeycomb lattice: structure, on-site spin-orbit coupling and spin polarization. Sci Rep, 2015, 5, 11512
[45] Liu M Y, Huang Y, Chen Q Y, et al. Strain and electric field tunable electronic structure of buckled bismuthene. RSC Adv, 2017, 7(63), 39546
[46] Pillai S B, Dabhi S D, Jha P K. Hydrogen evolution reaction and electronic structure calculation of two dimensional bismuth and its alloys. Int J Hydrogen Energ, 2018, 43(47), 21649
[47] Hu T, Hui X, Zhang X, et al. Nanostructured Bi grown on epitaxial graphene/SiC. J Phys Chem Lett, 2018, 9(19), 5679
[48] Huang H, Wong S L, Wang Y, et al. Scanning tunneling microscope and photoemission spectroscopy investigations of bismuth on epitaxial graphene on SiC(0001). J Phys Chem C, 2014, 118(43), 24995
[49] Wang Y, Chen K, Hao H, et al. Engineering ultrafast charge transfer in a bismuthene/perovskite nanohybrid. Nanoscale, 2019, 11(6), 2637
[50] Kumar P, Singh J, Pandey C A. Rational low temperature synthesis and structural investigations of ultrathin bismuth nanosheets. RSC Adv, 2013, 3(7), 2313
[51] Han N, Wang Y, Yang H, et al. Ultrathin bismuth nanosheets from in situ topotactic transformation for selective electrocatalytic CO_2 reduction to formate. Nat Commun, 2018, 9(1), 1320
[52] Wang L, Wang C, Li F, et al. In situ synthesis of Bi nanoflakes on Ni foam for sodium-ion batteries. Chem Commun, 2017, 54(1), 38
[53] Walker E S, Na S R, Jung D, et al. Large-area dry transfer of single-crystalline epitaxial bismuth thin films. Nano Lett, 2016, 16(11), 6931
[54] Zucchetti C, Dau M T, Bottegoni F, et al. Tuning spin-charge interconversion with quantum confinement in ultrathin bismuth films. Phy Rev B, 2018, 98(18), 184418
[55] Meyer D, Jnawali G, Hattab H, et al. Rapid onset of strain relief by massive generation of misfit dislocations in Bi(111)/Si(001) heteroepitaxy. Appl Phys Lett, 2019, 114(8), 081601
[56] He B C, Tian G, Gou J, et al. Structural and electronic properties of atomically thin bismuth on Au(111). Surf Sci, 2019, 679, 147
[57] Yang F, Miao L, Wang Z F, et al. Spatial and energy distribution of topological edge states in single Bi(111) bilayer. Phys Rev

Lett, 2012, 109(1), 016801
[58] Song F, Wells J W, Jiang Z, et al. Low-temperature growth of bismuth thin films with (111) facet on highly oriented pyrolytic graphite. ACS Appl Mater Interfaces, 2015, 7(16), 8525
[59] Nagao T, Sadowski J, Saito M, et al. Nanofilm allotrope and phase transformation of ultrathin Bi film on Si(111)-7 × 7. Phys Rev Lett, 2004, 93(10), 105501
[60] Sadowski J T, Nagao T, Yaginuma S, et al. Stability of the quasicubic phase in the initial stage of the growth of bismuth films on Si(111) -7 × 7. J Appl Phys, 2006, 99(1), 014904
[61] Wang X, Yang X, Shen N, et al. Atomistic insights into the growth of Bi (110) thin films on Cu (111) substrate. Appl Surf Sci, 2019, 481, 1449
[62] Rodil S E, Garcia-Zarco O, Camps E, et al. Preferential orientation in bismuth thin films as a function of growth conditions. Thin Solid Films, 2017, 636, 384
[63] Dauscher A, Boffoue M, Lenoir B, et al. Unusual growth of pulsed laser deposited bismuth films on Si(100). Appl Surf Sci, 1999, 138, 188
[64] Wu K S, Chern M Y. Temperature-dependent growth of pulsed-laser-deposited bismuth thin films on glass substrates. Thin Solid Films, 2008, 516(12), 3808
[65] Jankowski M, Kaminski D, Vergeer K, et al. Controlling the growth of Bi(110) and Bi(111) films on an insulating substrate. Nanotechnology, 2017, 28(15), 155602
[66] Yang L, Zheng Y X, Yang S D, et al. Ellipsometric study on temperature dependent optical properties of topological bismuth film. Appl Surf Sci, 2017, 421, 899
[67] Jaina R K, Kaura J, Aroraa S, et al. Effects of oblique angle deposition on structural, electrical and wettability properties of Bi thin films grown by thermal evaporation. Appl Surf Sci, 2019, 463, 45
[68] Kumari L, Lin S J, Lin J H, et al. Effects of deposition temperature and thickness on the structural properties of thermal evaporated bismuth thin films. Appl Surf Sci, 2007, 253(14), 5931
[69] El-Sayed N Z. Physical characteristics of thermally evaporated bismuth thin films. Vacuum, 2006, 80(8), 860
[70] Qin X F, Sui C Y, Di L X. Influence of substrate temperature on the morphology and structure of bismuth thin films deposited by magnetron sputtering. Vacuum, 2019, 166, 316
[71] Duan X, Yang J, Zhu W, et al. Structure and electrical properties of bismuth thin films prepared by flash evaporation method. Mater Lett, 2007, 61(22), 4341
[72] Bedoya-Hincapié C M, Roche J, Restrepo-Parra E, et al. Structural and morphological behavior of bismuth thin films grown through DC-magnetron sputtering. Rev chil ing, 2015, 23(1), 92
[73] Stanley S A, Stuttle C, Caruana A J, et al. An investigation of the growth of bismuth whiskers and nanowires during physical vapour deposition. J Phys D, 2012, 45, 435304
[74] Kim D H, Lee S H, Kim J K, et al. Structure and electrical transport properties of bismuth thin films prepared by RF magnetron sputtering. Appl Surf Sci, 2006, 252(10), 3525
[75] Takashiri M, Hamada J. Bismuth antimony telluride thin films with unique crystal orientation by two-step method. J Alloy Compd, 2016, 683, 276
[76] Takashiri M, Imai K, Uyama M, et al. Comparison of crystal growth and thermoelectric properties of n-type Bi–Se–Te and p-type Bi –Sb –Te nanocrystalline thin films: Effects of homogeneous irradiation with an electron beam. J Appl Phys, 2015, 115(21), 214311
[77] Kawakami N, Lin C L, Kawahara K, et al. Structural evolution of Bi thin films on Au(111) revealed by scanning tunneling microscopy. Phys Rev B, 2017, 96(20), 205402
[78] International roadmap for devices and systems (More Moore). 2018; Available from: https://irds.ieee.org/images/files/pdf/2017/2017IRDS_MM.pdf.
[79] Jing X, Illarionov Y, Yalon E, et al. Engineering field effect transistors with 2D semiconducting channels: Status and prospects. Adv Funct Mater, 2019, 30(18), 1901971
[80] Zhou W, Chen J, Bai P, et al. Two-dimensional pnictogen for field-effect transistors. Research, 2019, 2019, 1046329
[81] Jeon J, Jang S K, Jeon S M, et al. Layer-controlled CVD growth of large-area two-dimensional MoS_2 films. Nanoscale, 2015, 7(5), 1688
[82] Yang Z, Hao J, Yuan S, et al. Field-effect transistors based on amorphous black phosphorus ultrathin films by pulsed laser deposition. Adv Mater, 2015, 27(25), 3748
[83] Tao L, Cinquanta E, Chiappe D, et al. Silicene field-effect transistors operating at room temperature. Nat Nanotechnol, 2015, 10(3), 227
[84] Grazianetti C, Cinquanta E, Tao L, et al. Silicon nanosheets: Crossover between multilayer silicene and diamond-like growth regime. ACS Nano, 2017, 11(3), 3376
[85] Bhuvaneswari R, Nagarajan V, Chandiramouli R. Electronic properties of novel bismuthene nanosheets with adsorption studies of G-series nerve agent molecules – a DFT outlook. Phys Lett A, 2019, 383(33), 125975
[86] Maria J P, Nagarajan V, Chandiramouli R. Benzyl chloride and chlorobenzene adsorption studies on bismuthene nanosheet: A DFT study. J Inorg Organomet Polym Mater, 2019, 30(6), 1888
[87] Snehha P, Nagarajan V, Chandiramouli R. Novel bismuthene nanotubes to detect NH_3, NO_2 and PH_3 gas molecules – A first-principles insight. Chem Phys Lett, 2018, 712, 102
[88] Yao J D, Shao J M, Yang G W. Ultra-broadband and high-responsive photodetectors based on bismuth film at room temperature. Sci Rep, 2015, 5, 12320
[89] Zhou Q, Lu D, Tang H, et al. Self-powered ultra-broadband and flexible photodetectors based on the bismuth films by vapor deposition. ACS Appl Electron Mater, 2020, 2(5), 1254
[90] Lu L, Wang W, Wu L, et al. All-optical switching of two continuous waves in few layer bismuthene based on spatial cross-phase modulation. ACS Photonics, 2017, 4(11), 2852
[91] Chai T, Li X, Feng T, et al. Few-layer bismuthene for ultrashort pulse generation in a dissipative system based on an evanescent field. Nanoscale, 2018, 10(37), 17617
[92] Hicks L D, Harman T C, Dresselhaus M S. Use of quantum-well superlattices to obtain a high figure of merit from nonconventional thermoelectric materials. Appl Phys Lett, 1993, 63(23), 3230
[93] Cheng L, Liu H, Tan X, et al. Thermoelectric properties of a monolayer bismuth. J Phys Chem C, 2014, 118(2), 904
[94] Guo P, Li X, Chai T, et al. Few-layer bismuthene for robust ultrafast photonics in C-band optical communications. Nanotechnology, 2019, 30(35), 354002
[95] Lyeo H K, Cahill D G. Thermal conductance of interfaces between highly dissimilar materials. Phys Rev B, 2006, 73(14), 144301
[96] Gallo C F, Chandrasekhar B S, Sutter P H. Transport properties of bismuth single crystals. J Appl Phys, 1963, 34(1), 144
[97] Liao C N, Kuo S W. Thermoelectric characterization of sputter-deposited Bi/Te bilayer thin films. J Vac Sci Technol A, 2005, 23(3), 559
[98] Kim S I, Lee K H, Mun H A, et al. Dense dislocation arrays embedded in grain boundaries for high-performance bulk thermoelectrics. Science, 2015, 348(6230), 109
[99] Mishra S K, Satpathy S, Jepsen O. Electronic structure and thermoelectric properties of bismuth telluride and bismuth selenide. J Phys: Condens Matter, 1997, 9(2), 461
[100] Du Y, Cai K F, Li H, et al. Influence of sintering temperature on the microstructure and thermoelectric properties of n-type $Bi_2Te_{3-X}Se_X$ nanomaterials. J Electron Mater, 2011, 40(5), 518
[101] Hicks L D, Dresselhaus M S. Effect of quantum-well structures on the thermoelectric figure of merit. Phys Rev B, 1993, 47(19), 12727

[102] Hicks L D, Dresselhaus M S. Thermoelectric figure of merit of a one-dimensional conductor. Phys Rev B, 1993, 47(24), 16631
[103] Wu C Y, Sun L, Gong H R, et al. Influence of internal displacement on band structure, phase transition, and thermoelectric properties of bismuth. J Mater Sci, 2019, 54(8), 6347
[104] Xu Y, Gan Z, Zhang S C. Enhanced thermoelectric performance and anomalous seebeck effects in topological insulators. Phys Rev Lett, 2014, 112(22), 226801
[105] Das V D, Soundararajan N. Size and temperature effects on the Seebeck coefficient of thin bismuth films. Phys Rev B, 1987, 35(12), 5990
[106] Cho S, DiVenere A, Wong G K, et al. Thermoelectric power of MBE grown Bi thin films and Bi/CdTe superlattices on CdTe substrates. Solid State Commun, 1997, 102(9), 673
[107] Du H, Sun X, Liu X, et al. Surface Landau levels and spin states in bismuth (111) ultrathin films. Nat Commun, 2016, 7, 10814
[108] Gou J, Kong L, He X, et al. The effect of moiré superstructures on topological edge states in twisted bismuthene homojunctions. Sci Adv, 2020, 6(23), eaba2773
[109] Yang F Y, Liu K, Hong K, et al. Large magnetoresistance of electrodeposited single-crystal bismuth thin films. Science, 1999, 284(5418), 1335
[110] Wang N, Zhang L, Wang T, et al. Origin of linear magnetoresistance in polycrystalline Bi films. J Appl Phys, 2020, 127(2), 025105
[111] Wang N, Qi Y. Enhanced transport properties of Bi thin film by preferential current flow pathways in low angle grain boundaries. Vacuum, 2019, 169, 108874
[112] Xu Z X, Yan J M, Xu M, et al. Multistate resistance switching in Bi/PMN–PT(111) heterostructures by electric and magnetic field. J Mater Sci-Mater El, 2020, 31(4), 3585
[113] Kong X, Liu Q, Zhang C, et al. Elemental two-dimensional nanosheets beyond graphene. Chem Soc Rev, 2017, 46(8), 2127
[114] Guo S, Zhang Y, Ge Y, et al. 2D V-V binary materials: Status and challenges. Adv Mater, 2019, 31(39), 1902352
[115] Ueda Y, Duy Khang N H, Yao K, et al. Epitaxial growth and characterization of $Bi_{1-X}Sb_X$ spin Hall thin films on GaAs(111)A substrates. Appl Phys Lett, 2017, 110(6), 062401
[116] Cho S, DiVenere A, Wong G K, et al. Transport properties of Bi_{1-X}-Sb_X alloy thin films grown on CdTe(111)B. Phys Rev B, 1999, 59(16), 10691
[117] Smith G E, Wolfe R. Thermoelectric properties of bismuth-antimony alloys. J Appl Phys, 1962, 33(3), 841
[118] Linseis V, Völklein F, Reith H, et al. Thickness and temperature dependent thermoelectric properties of $Bi_{87}Sb_{13}$ nanofilms measured with a novel measurement platform. Semicond Sci Technol, 2018, 33(8), 085014
[119] Wu C Y, Sun L, Han J C, et al. Band structure, phonon spectrum, and thermoelectric properties of β-BiAs and β-BiSb monolayers. J Mater Chem C, 2020, 8(2), 581
[120] Zhang H J, Liu C X, Qi X L, et al. Topological insulators in Bi_2Se_3, Bi_2Te_3 and Sb_2Te_3 with a single Dirac cone on the surface. Nat Phys, 2009, 5(6), 438
[121] Adam A M, Elshafaie A, Mohamed A A, et al. Thermoelectric properties of Te doped bulk Bi_2Se_3 system. Mater Res Express, 2018, 5(3), 035514
[122] Ge Z H, Ji Y H, Qiu Y, et al. Enhanced thermoelectric properties of bismuth telluride bulk achieved by telluride-spilling during the spark plasma sintering process. Scripta Mater, 2018, 143, 90
[123] Zahid F, Lake R. Thermoelectric properties of Bi_2Te_3 atomic quintuple thin films. Appl Phys Lett, 2010, 97(21), 212102
[124] Guo D L, Hu C G. Ultrahigh thermoelectricity of atomically thick Bi_2Se_3 single layers: A computational study. Appl Surf Sci, 2014, 321, 525
[125] Sharma A, Srivastava A K, Senguttuvan T D, et al. Robust broad spectral photodetection (UV-NIR) and ultra high responsivity investigated in nanosheets and nanowires of Bi_2Te_3 under harsh nano-milling conditions. Sci Rep, 2017, 7(1), 17911
[126] Wang F, Li L, Huang W, et al. Submillimeter 2D Bi_2Se_3 flakes toward high-performance infrared photodetection at optical communication wavelength. Adv Funct Mater, 2018, 28(33), 1802707